AD-A141 271 THE INFLUENCE OF LATTICE IMPERFECTIONS ON THE CHEMICAL REACTIVITY OF SOLI..(U) UNIVERSITY OF STRATHCLYDE GLASGOW (SCOTLAND) DEPT OF PURE AND.. 1/1

UNCLASSIFIED J N SHERWOOD ET AL. FEB 84 DAERO-78-G-078 F/G 20/2 NL

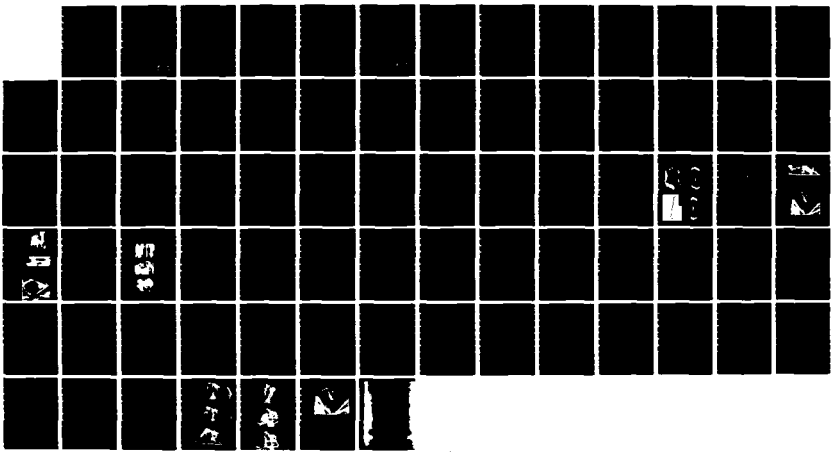

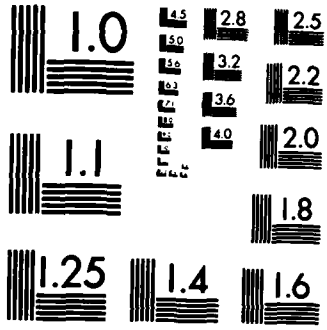

MICROCOPY RESOLUTION TEST CHART
NATIONAL BUREAU OF STANDARDS-1963-A

AD

(12)

THE INFLUENCE OF LATTICE IMPERFECTIONS ON THE CHEMICAL REACTIVITY OF SOLIDS

THE GROWTH, PERFECTION AND DEFECT PROPERTIES OF PETN AND RDX SINGLE CRYSTALS

by

John N. Sherwood
Peter J. Halfpenny
Kevin J. Roberts

FINAL REPORT (PART I)

FEBRUARY 1984

United States Army

EUROPEAN RESEARCH OFFICE FOR THE U.S. ARMY

London England

CONTRACT NUMBER DAERO-78-G-078

Professor John N. Sherwood
University of Strathclyde

Approved for Public Release; distribution unlimited

UNCLASSIFIED
SECURITY CLASSIFICATION OF THIS PAGE *(When Data Entered)*

REPORT DOCUMENTATION PAGE		READ INSTRUCTIONS BEFORE COMPLETING FORM
1. REPORT NUMBER	2. GOVT ACCESSION NO. AD A141211	3. RECIPIENT'S CATALOG NUMBER
4. TITLE *(and Subtitle)* The Influence of Lattice Imperfections on the Chemical Reactivity of Solids.		5. TYPE OF REPORT & PERIOD COVERED FINAL TECHNICAL
		6. PERFORMING ORG. REPORT NUMBER
7. AUTHOR(s) J. N. Sherwood		8. CONTRACT OR GRANT NUMBER(s) DAERC-78-G-078
9. PERFORMING ORGANIZATION NAME AND ADDRESS University of Strathclyde Department of Pure and Applied Chemistry Glasgow, G1 1XL, SCOTLAND		10. PROGRAM ELEMENT, PROJECT, TASK AREA & WORK UNIT NUMBERS 6.11.02A 1T16 1102BH57-02
11. CONTROLLING OFFICE NAME AND ADDRESS USARDSG (UK) Box 65 FPO, New York 09510		12. REPORT DATE FEBRUARY 1984
		13. NUMBER OF PAGES 137
14. MONITORING AGENCY NAME & ADDRESS(if different from Controlling Office) U. S. Army Research Office P. O. Box 12211 Research Triangle Park, NC		15. SECURITY CLASS. (of this report) UNCLASSIFIED
		15a. DECLASSIFICATION/DOWNGRADING SCHEDULE

16. DISTRIBUTION STATEMENT *(of this Report)*
Approved for Public Release; Distribution Limited
UN

17. DISTRIBUTION STATEMENT *(of the abstract entered in Block 20, if different from Report)*

18. SUPPLEMENTARY NOTES

19. KEY WORDS *(Continue on reverse side if necessary and identify by block number)*
Energetic materials, Detonation, PETN, RDX, HMX, Single crystals, Crystal growth, Crystal perfection, Dislocations, Mechanical properties, Dislocation slip, Twinning, Polymorphism, Mechanical deformation.

20. ABSTRACT *(Continue on reverse side if necessary and identify by block number)*
This report presents an assessment of the growth and perfection of single crystals of the secondary explosive materials PETN and RDX. An account is also given of some preliminary studies of their mechanical behaviour.

Details are presented for the preparation of large single crystals of PETN and RDX of extremely high perfection. Using the techniques of X-ray diffraction topography coupled where possible with theoretical calculations, an analysis is made of the dominant growth defect structure of these materials.
cont ...

DD FORM 1 JAN 73 1473 EDITION OF 1 NOV 65 IS OBSOLETE

UNCLASSIFIED
SECURITY CLASSIFICATION OF THIS PAGE *(When Data Entered)*

In both cases the principal defects are dislocations. There is also evidence of growth twinning in PETN. The character (line direction and Burgers vector) of the dislocations are defined. Burgers vectors up to and including lattice translations of <111> (PETN) and <110> (RDX) were identified.

Initial attempts have been made to examine the mechanical properties of PETN and RDX using microhardness indentation, etching techniques and X-ray topography. The results are used to make an appraisal of the likely dominant mechanical deformation processes. These are

PETN - microtwinning and dislocation slip on {110} slip planes, Burgers vector $\underline{b}$ [001].

RDX - dislocation slip on (010) (dominant) and possibly also on (011) or (021) and (001) slip planes, Burgers vectors on (010); b[100] and on (001); b[010] and b[110].

SUMMARY

This report presents an assessment of the growth and perfection of single crystals of the secondary explosive materials PETN and RDX. An account is also given of some preliminary studies of their mechanical behaviour.

Details are presented for the preparation of large single crystals of PETN and RDX of extremely high perfection. Using the techniques of X-ray diffraction topography coupled where possible with theoretical calculations, an analysis is made of the dominant growth defect structure of these materials. In both cases the principal defects are dislocations. There is also evidence of growth twinning in PETN. The character (line direction and Burgers vector) of the dislocations are defined. Burgers vectors up to and including lattice translations of <111> (PETN) and <110> (RDX) were identified.

Initial attempts have been made to examine the mechanical properties of PETN and RDX using microhardness indentation, etching techniques and X-ray topography. The results are used to make an appraisal of the likely dominant mechanical deformation processes. These are -

PETN - microtwinning and dislocation slip on {110} slip planes, Burgers vector $\underline{b}$[001].

RDX - dislocation slip on (010) (dominant) and possibly also on (011) or (021) and (001) slip planes, Burgers vectors on (010); b[100] and on (001); b[010] and b[110].

PART I

CONTENTS

REPORT

Studies of the Growth, Perfection and Defect Properties of Pentaerythritol tetranitrate (PETN) and Cyclotrimethylene Trinitramine (RDX)

1. The Crystal Growth and Perfection of Pentaerythritol Tetranitrate (PETN).

2. Characterisation of the Growth-Induced Dislocation Structure of Pentaerythritol Tetranitrate (PETN)

Comprising a series of five papers to be published under the series title DISLOCATIONS IN ENERGETIC MATERIALS. Each paper is separately numbered.

Part I contains the Introduction and first two papers.

Part II contains the remaining papers.

INTRODUCTION

It is accepted generally that the impact initiation of solid energetic materials occurs by the transfer of mechanical energy into heat within small volumes (hot spots) in the material. Despite this agreement on the potential source of the initiation, there is considerable controversy as to the basic mechanism by which the transfer of energy occurs.

Field [1-3] has summarized the possible macroscopic mechanisms by which this might occur as:

(i) Adiabatic compression of trapped gas spaces.

(ii) Viscous heating of material rapidly extruded between impacting surfaces or grains.

(iii) Friction between the impacting surfaces, and/or the explosive crystals, and/or grit particles in the explosion layer.

(iv) Localised adiabatic shear of the materials during failure.

The role of macroscopic mechanical deformation of the explosive is inherent in all of these mechanisms. It has been emphasized by more specific experiments. For example, Kholevo [4] has shown that the sensitiveness of explosives to impact initiation can be reduced if the sample is prevented from flowing. Also, Heavens and Field [1] and Field, Swallowe and Heavens [3] have shown that plastic flow and even melting does occur during impact initiation. The last study also demonstrated that initiation can occur following fragmentation or melting of the solid and not necessarily in the bulk crystalline state.

Encouraged by information of this type, several workers have proposed mechanical mechanisms for the build up of energy. Afanasev and Bobolev [5] suggested a fracture based mechanism in which 'hot spots' are formed by the release of energy along slip surfaces at the onset of gross mechanical failure. At the more microscopic level, Fox and Soria-Ruiz [6,7] have shown that high temperatures can indeed be generated at the tips of moving cracks and have suggested that this could lead to initiation. Field and his co-workers [3] reject this single crack theory on the basis that the energy produced is too low to give the necessary temperature and size of 'hot spot'. They do note, however, that the energy of fracture can cause chemical decomposition to gaseous products which in turn could be adiabatically compressed to yield ignition. Thus a mechanical basis remains.

An alternative microscopic approach taken by Coffey [8], Coffey and Armstrong [9] and by Elban and Armstrong [10] is to associate dislocation motion with initiation. They propose that the impact causes dislocations to be driven along slip planes until they pile up against some obstacle. The sudden transfer of kinetic to potential energy then generates the hot spot. This theory again suffers from the problem that the energy gained is low and the volume heated will be small when compared with the anticipated hot spot size.

Despite this potential involvement of mechanical deformation in the initiation process, there has been little attempt to investigate and define the nature and properties of lattice defects in energetic materials, their role in micro-plasticity and the relationship of this to macro-plasticity and hence initiation. The present series of studies was commenced in an effort to redress this situation. Such information is also useful, however, in relation to the changes which might occur in the development of sub-structures in energetic materials during storage and thermal treatment. For example, such changes may yield voids or gas spaces which could influence the sensitivity of the stored material. It is also relevant to the general mechanical behaviour of such solids in preparation and packing.

1. Basis and Progress of Programme

The principal aims of the programme were (1) to examine and define the nature and properties of the commonly occurring lattice defects in organic secondary explosive materials and (2) to assess the role of these defects in crystal growth and in the microplasticity of the solid.

1.1 Experimental techniques

The method chosen for the detailed studies of the dislocation structure was X-ray topography.[11] This technique has the advantage that it can be used for the characterisation of the bulk defect structure of large samples (1cm^3) provided that

they are of high quality ($<10^{-5}$ dislocations cm^{-2}). It can also be used under ambient conditions with sensitive or reactive materials which could decompose under more extreme conditions, for example in the high electron fluxes of the electron microscope.

The examination can readily be extended to detailed studies of the microplasticity of the materials using stress/strain stages designed to fit the X-ray topographic camera. This allows the behaviour of the defects to be examined 'in situ' under stress and their development assessed.

In addition to the above, and to provide complementary evidence on mechanical behaviour, studies of bulk deformation were carried out by microhardness indentation and dislocation etching techniques.

1.2 Materials

The materials chosen for examination in the full programme were

Pentaerythritol tetranitrate (PETN)

Cyclotrimethylene trinitramine (RDX)

Trinitrotoluene (TNT)

Cyclotetramethylene Tetranitramine (HMX)

Nitroguanidine (NQ)

Diamino trinitrobenzene (DATB)

Triamino trinitrobenzene (TATB)

1.3 Summary of progress

For this type of examination, a necessary prerequisite is the availability of large, high quality, single crystals. Consequently, a considerable part of the initial contract was devoted to the determination of conditions required for the production of such crystals. Satisfactory procedures have been developed for the production of large (5-10cm^3) highly perfect crystals of PETN, RDX, TNT and HMX.

Of these, TNT proved to be the most difficult to grow due to the high initial impurity content, polymorphism and ready occurrence of twinning during growth of this material. The last two factors were studied in some detail and the solid and its crystallization characteristics were defined for the first time.

Only limited success was achieved with the remaining materials due predominantly to their lower solubilities. Of these NQ was grown in sizes up to 5x1x1mm^3. The crystals formed ragged needles and were unsuitable for topography. DATB grew as clusters of rod-like and prismatic crystals from DMSO solution in sizes up to 5x5x2mm^3 but only after rigorous purification. Often, a DATB/DMSO complex crystallized rather than the pure material. The occurrence of this complex seemed to depend on the rate of growth of the crystal. TATB did not yield crystals on crystallization.

For the four principal materials the growth defect structure was defined by the technique of X-ray transmission topography using both monochromatic laboratory sources and the polychromatic synchrotron radiation source. The latter proved to be most useful in defining the existence of and monitoring the removal of multiple twinning during growth in TNT.

From the above topographic assessment, it proved possible to define the potential dominant dislocation slip systems in RDX and PETN and to show that the dominant deformation mechanism in TNT should occur by mechanical twinning. These assessments were supplemented by microhardness indentation and etching studies in PETN and RDX.

At the present time, all data on PETN and RDX have been fully analysed and are presented here in the form of papers prepared for publication. This probably represents the most concise method of reporting this work. A more detailed account is available in the Doctoral Thesis of P.J. Halfpenny (University of Strathclyde 1982).

Due to the more complicated nature of TNT, work on this material was incomplete at the end of the initial contract. The work has continued in the interim. A summary of the work achieved to date on this material is presented in the final report on contract DAJA37-81-M-0395 which is submitted simultaneously with this report.

1.4 Future work

The definition of the methods for the preparation of good single crystals of these energetic materials and the definition of their defect structure now opens the way for the examination of the micro-plasticity of these solids and other defect associated processes. Studies of this kind form the major basis of the continuing programme.

REFERENCES

1. S.N. Heavens and J.E. Field, Proc. Roy. Soc., A338, 77 (1974).

2. G.M. Swallowe and J.E. Field, Proc. Roy. Soc., A379, 389 (1982).

3. J.E. Field, G.M. Swallowe and S.N. Heavens, Proc. Roy. Soc., A382, 231 (1982).

4. N.A. Kholevo, Trudy Kazan. Khim. Tech. Inso., 10, 91 (1946).

5. G.T. Afanasev and V.K. Bobolev, Initiation of Solid Explosives by Impact, Israel Program for Scientific Translations, Jerusalem 1971.

6. P.G. Fox and J.Soria Ruiz, Proc. Roy. Soc., A317, 79 (1970).

7. P.G. Fox, J. Solid State Chem., 2, 491 (1970).

8. C.S. Coffey, Phys. Revs., B24 (1981).

9. C.S. Coffey and R.W. Armstrong, Shock Waves and High Strain Rate Phenomena in Metals: Concepts and Applications, Editors M.A. Mayer and L.E. Muir (Plenum, New York) 1981, p. 313.

10. W.L. Elban and R.W. Armstrong, 7th International Symposium on Detonation, Annapolis, Maryland (US Office of Naval Research) 1981.

11. B.K. Tanner and D.K Bowen, Editors 'Studies of Growth Defects in Crystals using X-Ray Methods', NATO-ASI No. B63, Durham, UK, 1979, Plenum, NY 1980.

DISLOCATIONS IN ENERGETIC MATERIALS

1. The Crystal Growth and Perfection of Pentaerythritol Tetranitrate (PETN)

P.J. Halfpenny*, K.J. Roberts+ and J.N. Sherwood

Department of Pure and Applied Chemistry

University of Strathclyde

Glasgow G1 1XL

Scotland

*Engineering Materials Laboratories, The University, Highfield, Southampton SO9 5NH

+Institut fur Kristallographie, Rhein.-Westf. Technische Hochschule, 5100 Aachen, FRG

ABSTRACT

Crystals of the secondary explosive material pentaerythritol tetranitrate (PETN) were grown from ethyl acetate and from acetone solutions by temperature lowering and solvent evaporation techniques. The growth-induced defect structure revealed by X-ray topography was found to consist of growth bands, growth sector boundaries, dislocations and solvent inclusions. All of the crystals grown exhibited only the forms {110} and {101} with the former dominating. Additional growth sectors were revealed by topography and were found to correspond to {111} facets which had grown out in the early stages of growth. The crystal perfection was found to increase with more accurate control of growth conditions. In general the {110} growth sectors exhibited a higher defect density than the {101} sectors. This can be explained on the basis of the relative growth rates of the habit faces and the nature of the growth dislocations present.

1. INTRODUCTION

The important influence of lattice defects and crystal perfection upon the chemical reactivity of solids is well-established [1-3]. In the case of energetic solids it has also been suggested that dislocations are involved in the impact initiation of these materials due to the formation of localized 'hot spots' during plastic deformation. Such influences are of particular significance in the case of secondary energetic solids such as pentaerythritol tetranitrate (PETN).

PETN ($C(CH_2NO_2)_4$) crystallizes in the tetragonal space group $P\bar{4}2_1c$ with a = b = 0.938nm, c = 0.67nm and two molecules per unit cell.[4] It is highly sensitive to impact and also undergoes thermal decomposition below its melting point.[5] Consequently, its defect properties and their relationship with bulk properties, are of of particular interest.

The growth of single crystals of PETN from acetone solution has previously been reported by Koch.[6] Crystals up to 180g in weight were obtained by growth from seeded solutions using the temperature lowering, solvent evaporation and temperature difference methods. Tranchant [7] described the crystallization of PETN from acetone, ethyl acetate, nitromethane, ethanol and mixtures of the latter two solvents. It was found that evaporation of a solution of PETN in ethyl acetate yielded crystals of an equant habit while growth from the other solvents gave elongated prisms or tablets. Booth and Llewellyn [5] obtained

crystals of PETN from acetone exhibiting the forms {110} and {101}. None of these reports defined the perfection of the crystals obtained.

In this paper we report in detail on the growth of high quality single crystals of PETN and define, for the first time, the growth-induced defect structure as revealed by X-ray topography.[8]

2. CRYSTAL GROWTH

2.1 Growth Techniques and Apparatus

PETN (purity 99.75%) was recrystallized twice from distilled acetone before use. The single crystals were grown from saturated solutions [9] at, or slightly above, ambient temperature using either temperature lowering or solvent evaporation to produce the necessary supersaturation. The apparatus used is illustrated in Figure 1. The solution was contained in a long necked flask (A) fitted with a B45 or B60 ground glass seal and a stirring gland ST10/2 (Quickfit) (B). For growth by temperature lowering the flask was sealed to prevent evaporation of the solvent. The solution was stirred by a glass paddle (C) fitted with a hook or loop from which the seed crystal was suspended. The growth flask was surrounded by a 20 litre water bath (D) heated by an infrared lamp (E). The water bath was stirred continuously. Accurate temperature control was achieved using a long range contact thermometer (F). A synchronous motor (G) was used to drive down the contact of the thermometer thus lowering the temperature. The rate of temperature lowering could be varied by using motors of

different speeds and by using a time-sharing cam switching system [9] to provide a fine control of the temperature lowering rate. For crystal growth by solvent evaporation the temperature was held constant and the solvent allowed to evaporate by way of a limiting vent from the growth flask to the outside atmosphere.

2.2 Growth Conditions

Previous experience [9] of crystal growth of a wide range of materials from low temperature solution has indicated that the optimum conditions for growth are usually found within the following range:

a) Solubility; 20 to 100g of solution per 100g of solvent.

b) The ratio of solubility-temperature gradient to solubility; 0.01 to $0.03K^{-1}$.

In this study, crystals of PETN were grown from acetone and ethyl acetate solvents. The solubilities of PETN in these solvents at 293K are 24.8 and 10.6g per 100g of solvent [10] respectively with a solubility ratio of approximately $0.03K^{-1}$ in each case.

The growth parameters were varied in different growth experiments in order to determine the optimum conditions for preparation of high quality single crystals. The temperature was lowered at rates from $0.01Khr^{-1}$ up to $0.05Khr^{-1}$ over the temperature range 298 to 323K. Crystals were grown in both stirred and unstirred solutions. Stirring rates of between 10 and 60rpm were employed with a reverse in direction approximately every 20 to 30 seconds. The majority of seed crystals were suspended on fine glass rods. In some runs, however, the glass was replaced by nylon thread.

2.3 Results of Crystal Growth

All the crystals of PETN grown in this study exhibited only the forms {110} and {101}, irrespective of solvent or growth conditions. The crystal habit, however, varied significantly ranging from acicular (Figure 2a) to tabular (Figure 2b). Most of the crystals, however, were of the bulky prismatic habit shown in Figures 2c and 2d. The largest of the crystals was 35 x 13 x 10mm^3 and weighed approximately 15g.

Initial growth of the seed crystal invariably resulted in the formation of inclusions at the seed-crystal interface. In addition, defective regions frequently occurred around the seed suspending fibre. The deformed regions became more extensive with increased stirring rates and with the use of glass rather than nylon seed-suspending fibre. In both cases, however, the damage was confined to the immediate vicinity of the seed and seed rod leaving the remaining volume clear and of good optical quality.

Full details of the crystal growth experiments are summarized in Table 1.

3. CRYSTAL PERFECTION

3.1 X-ray Topography

The initial topographic examination of PETN crystals was directed towards establishing the general types of defects present together with an assessment of crystal perfection as a function of growth conditions.

Crystals were sectioned using a solvent saw and then polished on a solvent soaked cloth to remove surface damage. Cyclohexanone was found to be the most effective solvent for both slicing and polishing. The {110} slice plane was used extensively throughout the study. This orientation was found to afford an excellent view of defects in both the {110} and {101} growth sectors. Some (001) slices were examined. These were less suitable, especially for observing growth dislocations.

Copper $K\alpha_1$ radiation (0.154nm) was used for all topographs, which were recorded on Agfa Structurix D4 film. For this wavelength the linear absorption coefficient, μ, of PETN is $1.64 \times 10^3 m^{-1}$. The typical slice thicknesses were between 0.5 and 3mm. The product μt was therefore in the range 0.8 to 5. Thicknesses of about 1mm giving $\mu t = 1.5$ were more typical of the samples studied.

3.2 Growth defects in PETN

X-ray topographic studies of nearly perfect crystals grown from solution have shown [11-13] the basic growth-induced defect structure to include: growth sector boundaries, growth bands, inclusions and dislocations. This expected defect structure was also observed in PETN.

3.2.1 Growth sector boundaries

From the morphology of the crystal we can see that there are likely to be three types of growth sector boundaries. These types, shown schematically in Figure 3, are:

Type A representing the boundary between two of the {110} forms.

Type B representing the boundary between one sector of the {110} form and one of the {101} form.

Type C representing the boundary between two of the {101} forms.

The growth sector boundaries show both kinematical contrast and fringe contrast. The latter is characteristic of either a slight orientational mismatch between the lattice on either side of the boundary or of the incorporation of a thin layer of impurity molecules at the boundary. Similar contrast effects have been observed in crystals of salol and benzil.[13] In view of the disparity between the growth rates of the two forms, we would expect type B boundaries to exhibit the most lattice strain. However the observed variations in boundary contrast are, we believe, due primarily to differences in overall crystal perfection or in the angle from which the boundary is effectively viewed by the topograph. This latter case is illustrated in Figure 7 by type B boundaries which show either fringe or kinematical contrast depending on the orientation of the boundary with respect to the slice plane. These two factors effectively mask any differences in strain at the boundary caused by the different growth rates of the {110} and {101} forms.

3.2.2 Growth bands

Growth bands (labelled E) can be seen aligned normal to the growth directions in the {101} sectors in Figure 5. These were probably caused by small fluctuations in the growth conditions of the crystal yielding variations in lattice strain or solvent inclusion. The resulting bands of solvent are visible in X-ray topographs by virtue of the consequent change in lattice parameter.

3.2.3 Inclusions

In addition to growth bands, relatively large volumes of impurity can often become included into the growing crystal. Solvent inclusions are again the most common manifestation of this type of defect in solution grown crystals. During growth, solvent inclusions are attributable [14] to sudden variations in growth conditions resulting either in very rapid growth or in dissolution followed by regrowth. In the latter case, dissolution gives rise to a rounded surface on which terraces develop parallel to the habit faces. Here, solvent is readily entrapped until the terraces meet and a crystal edge is formed again. Even in the most carefully grown crystals, inclusions are almost invariably formed at the seed-crystal interface. This is due either to mechanical damage on the seed surface or to dissolution of the surface before growth begins. Solvent inclusions in PETN (labelled I) can be seen in Figure 5. As the crystal grows over an inclusion, closure mistakes and lattice misorientation inevitably occur. These can give rise to defects which continue to propagate as the crystal grows. The inclusions in Figure 5 generate two

types of defect; dislocations, definable by their contrast and direction of propagation towards the boundary facet, and other planar defects, P, propagating parallel to [001]. The line directions of the latter are not characteristic of any predicted dislocation system. Close examination reveals these defects to consist of a planar area bounded by lines of darker contrast (dislocations?). This coupled with the fact that they show a lowering of contrast in reflections with $\underline{g}$ having a component in the [001] direction leads us to speculate that they are twin lamellae. Thus we conclude that the mechanical deformation of this solid can occur by either dislocation migration or twin formation. Supplementary evidence for twin formation was also obtained from optical microscopy of compressively deformed specimens.

3.2.4 Dislocations

The dislocations observed in as-grown crystals of PETN were, almost without exception, straight and tended to follow a number of discrete, well-defined, line directions. Few of these line directions were low-indexed. Such characteristics are typical of growth-induced dislocations. Indeed, throughout the study, little evidence was found of mechanically induced dislocations in as-grown crystals. The characterization of dislocations in PETN together with a theoretical analysis of growth dislocation families will be given elsewhere [15,16]. The observed growth-induced dislocation types are summarized in Table 2. Typical dislocation densities varied between 10-10^3 lines cm^{-2}.

3.3 Influence of Growth Conditions on Crystal Perfection

The topographs shown in Figures 5, 7 and 8 illustrate the variation in crystal perfection with growth conditions.

The crystal shown in Figure 7 was grown from acetone by rapid, uncontrolled solvent evaporation. The defect density in this sample is so high that the strain fields overlap, preventing clear resolution of individual defects. The crystal is also warped as can be seen from the out-of-contrast region (labelled K).

Slower growth from acetone solution by solvent evaporation yielded crystals of considerably higher quality, as shown by Figure 5. The growth sector boundaries (labelled B) are very strongly contrasted which indicates that relatively large misorientations and/or strains are present. The heavy growth banding in the {101} sectors reflects the fluctuations in the rate of solvent evaporation. These sectors are, however, relatively free of large solvent inclusions. As a consequence they have a low dislocation density and large volumes are essentially dislocation free. In contrast to this the {110} sectors are much more defective with a high dislocation density. The greater perfection of the {101} sectors relative to the {110} sectors was common to all of the crystals examined.

Under rigorously controlled conditions of growth by slow cooling, PETN crystals of very low defect density were prepared. The topograph in Figure 8 shows a crystal grown from ethyl acetate by slow cooling at a rate of $0.008 K hr^{-1}$. The growth sector boundaries are still very prominent. Careful control of the growth

conditions resulted in a complete absence of growth bands and a low incidence of solvent inclusions, particularly in the {101} sectors. One large fluctuation has however produced the band of solvent inclusions (labelled L) parallel to the (110) crystal face. The dislocation density is again lower in the {101} sectors than in the {110} sectors. The low defect density and overall perfection of the crystal is demonstrated by the observation of well-defined Pendellosung fringes at the edges of the sample.

4. DISCUSSION

4.1 Morphology

The crystal growth of PETN has, despite the use of different solvents and/or growth conditions, yielded crystals exhibiting the forms {110} and {101} only. The law of Donnay and Harker [17] predicts that lattice planes having the largest interplanar spacing and therefore the smallest reticular area will form the predominant crystal faces. Although a relatively simple model, this approach explains important aspects of the morphology and perfection of PETN crystals. The reticular areas for low indexed planes in PETN were deduced by computer programme [18] and are listed in Table 3. It can be seen that the two smallest reticular areas correspond to the observed habit faces {110} and {101}. This observed crystal morphology is compatible with the more rigorous PBC approach [19]. In PETN the two non-equivalent molecules are centred at the origin and at body-centre positions in the unit cell. This packing results in a strong <111> PBC consistent with

dominant {110} and {101} forms (i.e. each of these forms has two <111> PBC's in the slice plane and is thus, under Hartman's notation [19], a crystallographically smooth F-face).

Although no other habit faces were observed on the 'as grown' crystals, 'extra' growth sectors were revealed in X-ray topographs. These sectors do not correspond to either of the above forms. They are instead associated with more rapidly growing faces which grow out in the early stages of growth and thus were never observed in the final crystals. In Figure 5 the extra growth sector, seen on the topograph taken ofa (110) slice, exhibits growth banding parallel to [110]. The corresponding growth face must therefore also lie in the [110] zone. Of the planes consistent with this observation, (111) has the smallest reticular area. This assignment is confirmed by the orientation of the four 'extra' growth sectors, seen on the topograph taken of an (001) slice, shown in Figure 6. All other possible habit faces have reticular areas much greater than those of the observed faces, thus accounting for the absence of other forms.

Variations in habit can result from two causes; solvent effects and the influence of mechanical damage induced following the capping of the seed crystal. The surface entropy factor α [20,21] is an important parameter in assessing the influence of solvent on morphology [22,23]. Human et al [22] have used the following relationship to assess this parameter for growth from a two component solution

$$\alpha_{hkl} = \xi_{hkl}(\Delta H_f/kT - \ln.x) \qquad (1)$$

where ξ_{hkl} is the anisotropy factor for a given face and which is related to the surface bond energy and ΔH_f is the heat of fusion. For PETN, ΔH_f= 48kJ mol^{-1} and x, the mole fraction of solute, is 4.3×10^{-2} and 2.9×10^{-2} for acetone and ethyl acetate solutions respectively at 293K.[10] Substitution of these figures into equation (1) yields $\alpha_{hkl} = 21.9\ \xi_{hkl}$ and $22.3\xi_{hkl}$ for the two solvents respectively. The similarity between these figures suggests that there should be little obvious difference in solvent effects and that mechanical damage will dominate. This likelihood is well-defined by the regular appearance of strongly defined strained volumes around the seed suspension rod as can be noted in Figure 2d. The influence of this on morphology should be random but as noted above, it decreased with a more plastic suspension fibre (e.g. nylon) and with less vigorous stirring rates. Both factors presumably cause less strain on the forming crystal.

4.2 Perfection

The influence of greater stability of growth conditions on the crystal perfection has already been illustrated by the elimination of growth banding, and a reduction in solvent inclusions and in dislocation density with the use of accurately controlled temperature lowering. In addition the morphology of the crystals plays an important role in defining the perfection of PETN particularly in the {101} growth sectors. The growth rate of the {101} forms being greater than that of the {110} forms tends to produce growth sector boundaries (of type B) which lie at shallow

angles (typically <30°) to [001]. The main dislocation types in {101} sectors propagate at angles between 34-58° to [001]. Thus there is a tendency for dislocations formed in the early stages of growth to refract into the {110} growth sectors (see Figure 9) as growth proceeds. The dislocation content in the {101} sectors then decreases with increasing growth period. This is well illustrated in Figure 10. This shows topographs taken from (001) slices cut from the 'cap', from between the 'cap' and seed regions and from the seed regions of a PETN crystal. Similar effects have been observed in other crystals which exhibit forms of differing growth rates, for example crystals of the KDP/ADP family [24,25]. As well as this 'refraction' of dislocations between growth sectors, growth dislocations were frequently observed to nucleate on the growth sector boundaries. In this circumstance and again due to their line direction, propagation was often only possible in {110} growth sectors.

5. CONCLUSIONS

Large single crystals (typically 35 x 13 x 10mm^3) of good optical quality can be prepared from low temperature solution using acetone and ethyl acetate solvents. The crystals normally exhibit a prismatic habit, with the as-grown crystals having well -defined {110} and {101} forms. The {111} form is also sometimes present in the early stages of growth. The defect structure comprises growth bands and sector boundaries, solvent inclusions, dislocations (density 10-10^3 lines cm^{-2}) and twin lamellae. The dislocations predominate in the {110} sectors due both to the refraction of the

mixed character, growth induced, dislocations from the {101} growth sectors into the {110} sectors and the increased entrapment of solvent inclusions in these sectors.

ACKNOWLEDGEMENTS

We express our grateful thanks to the European office of the US Army (USARDSG-UK) for their financial support of this work.

REFERENCES

1. J.M. Thomas,Adv. in Catalysis 19 (1969) 293.
2. I.D. Begg, P.J. Halfpenny, R.M. Hooper, R.S. Narang, K.J. Roberts and J.N. Sherwood, Proc. Roy. Soc. Lond. A (1983).
3. P.G. Fox and J. Soria-Ruiz, Proc. Roy. Soc. Lond. A 314 (1970) 429.
4. A.D. Booth and F.J. Llewellyn, J. Chem. Soc. (1947) 837.
5. W.L. Ng, J.E. Field and H.M. Hauser, J. Chem. Soc. Perkin II 6 (1976) 637.
6. E.W. Koch, Einfuhrungssymp. Inst. Chem.-Tech. Unters (1973) 478.
7. J. Tranchant, Mem. Poudres 34 (1952) 117.
8. A.R. Lang, 'Modern Diffraction and Imaging Techniques in Materials Science' Eds. Amelinckx et al. North-Holland (1978) p623.
9. R.M. Hooper, B.J. McArdle, R.S. Narang and J.N. Sherwood, 'Crystal Growth' 2nd. Edn., Ed.B. Pamplin, Pergamon (1975) p395.
10. R.N. Roberts and R.H. Dinegar, J. Phys. Chem. 62 (1958) 1009.
11. A.R. Lang, 'Crystal Growth: an Introduction', Ed. P. Hartman, North Holland (1973), p444.
12. A. Authier, 'Crystal Growth and Materials', Eds. E. Kaldis and H.J. Scheel, North Holland (1976) p516.
13. H. Klapper, 'Characterization of Crystal Growth Defects by X-ray Methods', Ed. B.K. Tanner and D.K. Bowen, Plenum New York (1980) P122.

14. A.A. Chernov and D.E. Temkin, 'Crystal Growth and Materials', Eds. E. Kaldis and H.J. Scheel, North Holland (1977) p4.

15. P.J. Halfpenny, PhD. Thesis, University of Strathclyde (1982).

16. P.J. Halfpenny, K.J. Roberts and J.N. Sherwood, in preparation.

17. J.D.H. Donnay and D. Harker, Amer. Miner. 22 (1937) 446.

18. E. Dowty, Amer. Miner. 61 (1976) 448.

19. P. Hartman, 'Crystal Growth: an Introduction', Ed. P. Hartman, North Holland (1973) p367.

20. K.A. Jackson, 'Liquid Metals and Solidification', (American Society for Metals, Cleveland, 1958) p174.

21. P. Bennema and G.H. Gilmer, 'Crystal Growth: an Introduction', Ed. P. Hartman, North Holland, Amsterdam 1973, P623.

22. J.R. Bourne and R.J. Davey, J. Crystal Growth, 36 (1976) 278.

23. H.J. Human, J.P. van der Eerden, L.A.M.J. Jettin and J.G.M. Odekerken, J. Crystal Growth, 51 (1981) 589.

24. H. Klapper, Y.M. Fishman and U.G. Lutsau, Phys. St. Solidi (Sa) 21 (1974) 115.

25. H.L. Bhat, K.J. Roberts and J.N. Sherwood, J. Applied Cryst. (1983), in press..

TABLE 1

GROWTH CONDITIONS AND DIMENSIONS OF PETN CRYSTALS

Crystal	Stirring r.p.m.	Solvent	Growth Method	Average Temperature Lowering Rate Khr^{-1}	Temp Range K	Dimensions [001] mm	[110] mm	[1$\bar{1}$0] mm	Comments
1	-	A	E	-	~293	24	14	5	Unseeded
2	60	E	C	0.04	319 303	20	5	5	
3	60	E	C	0.01	308 302	20	11	8	
4	60	E	C	0.03	315 307	30	10	7	
5	20	E	C	0.008	316 314	26	13	7	Considerable solvent evaporation occurred
6	60	E	C	0.02	309 298	35	5	8	
7	60	E	C	0.009	312 306	22	4	4	
8	60	A	C	0.006	303 301	21	6	5	
9	60	A	C	0.02	302 298	28	10	6	
10	-	A	C	0.009	302 297	27	2	2	
11	10	E	C	0.04	310 300	36	13	10	Nylon seed thread
12	-	E	C	0.01	306 298	30	9	10	Nylon seed thread

Note: 1) Solvent A = acetone, E = ethyl acetate.
2) E = solvent evaporation, C = slow cooling.
3) Seed rod is parallel to [110].

TABLE 2 OBSERVED GROWTH DISLOCATION TYPES IN PETN

Type	Growth sector	Burgers vector	Line Energy $eVnm^{-1}$	Character	Angle between [001] and line direction
1a	{110}	[001]	19	Edge	90.0
2a	{110}	<100>	35	Mixed	90.0
5a	{110}	<111>	84	Mixed	67.5
1b	{101}	[001]	18	Mixed	34
2b	{101}	<100>	35	Mixed	58
3c	{101}	<011>	52	Mixed	40
4c	{101}	<110>	81	Mixed	49.5
5c	{101}	<111>	87	Mixed	47.0

TABLE 3

THE RETICULAR AREAS OF CRYSTAL FACES

IN PETN-

No	Form	Reticular area (s/b^2)	Interplanar spacing (nm)
1	{110}	1.010	0.6632
2	{101}	1.229	0.5452
3	{111}	1.421	0.4714
4	{100}	1.429	0.938
5	{210}	1.597	0.4195
6	{201}	1.744	0.3842

FIGURE CAPTIONS

Figure 1 Schematic diagram of the crystal growth apparatus

Figure 2 A selection of PETN crystals grown from:

a) Acetone solution by temperature lowering (scale mark 5mm).

b) Acetone solution by solvent evaporation showing the influence of mechanical damage on the crystal morphology (scale mark 5mm).

c) Ethyl acetate solution by temperature lowering (scale mark 10mm).

d) Ethyl acetate solution by temperature lowering showing the strain which develops round a glass supporting rod (scale mark 10mm).

Figure 3 Schematic diagram of growth sectors and growth sector boundaries in a PETN crystal showing the three basic types of boundary.

Figure 4 Growth sector boundaries of types A and B showing the distinctive fringe contrast (scale mark 1mm)

Figure 5 X-ray topograph (220) reflection of a (110) slice cut from the crystal shown in Figure 2b (crystal 1, table 1) showing the extra (111) growth sector, D, growth sector boundaries types B, growth horizons E, solvent inclusions I and possible twin lamellae, P (scale mark 1mm).

Figure 6 A portion of a topograph 220 reflection of a (001) section of PETN (Figure 10b) showing four (111) growth sectors, D, at an early stage of growth (scale mark 1mm).

Figure 7 A 220 topograph of a complete crystal grown by rapid, uncontrolled, solvent evaporation showing the high density of dislocations and distortion which results under these conditions (B, growth sector boundary, K, portion of crystal twisted out of contrast) (scale mark 1mm).

Figure 8 Topograph of a (110) crystal slice of a crystal grown by temperature lowering from ethyl acetate solution under well-controlled conditions (crystal 5, table 1). (B, C, growth sector boundaries, L, solvent inclusions) (scale mark 1mm).

Figure 9 The projected line directions of growth induced dislocations in the {101} growth sector of PETN crystals showing how they will propagate towards and refract into the {110} sector.

Figure 10 Series of X-ray topographs taken from 'cap' region (X), from the region between 'cap' and seed (Y) and from the seed region (C) of crystal 3 (Table 1). Slice plane is (001), reflection 220.

(scale mark 1mm).

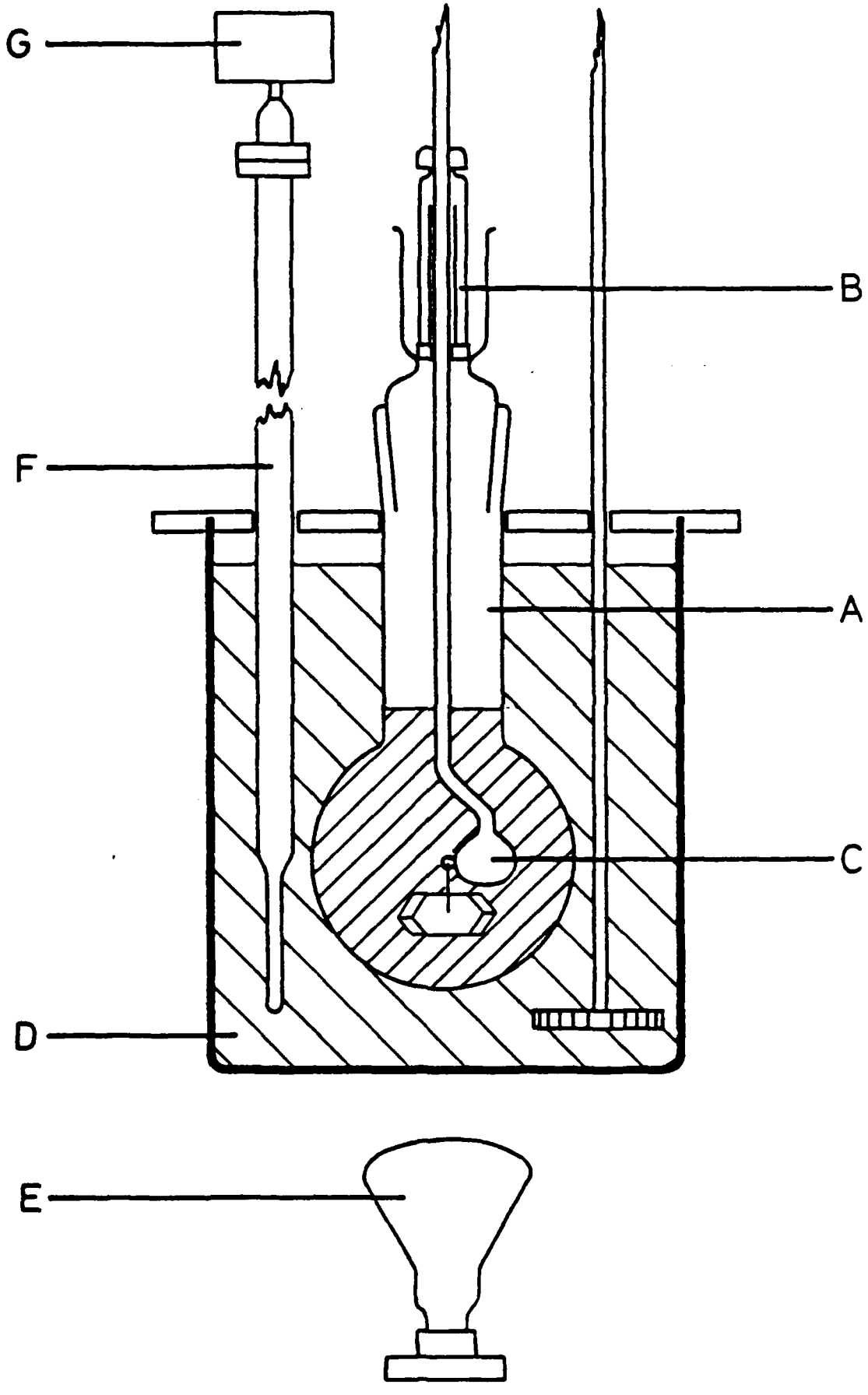

FIGURE 1

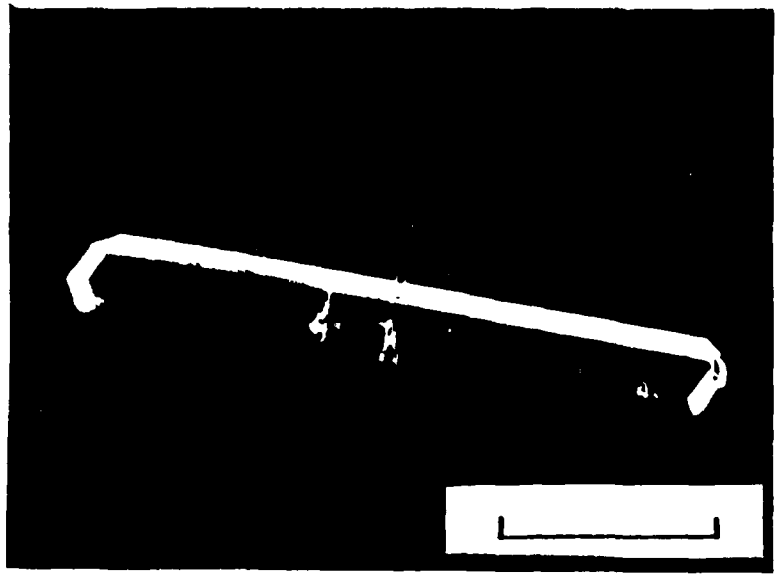

a

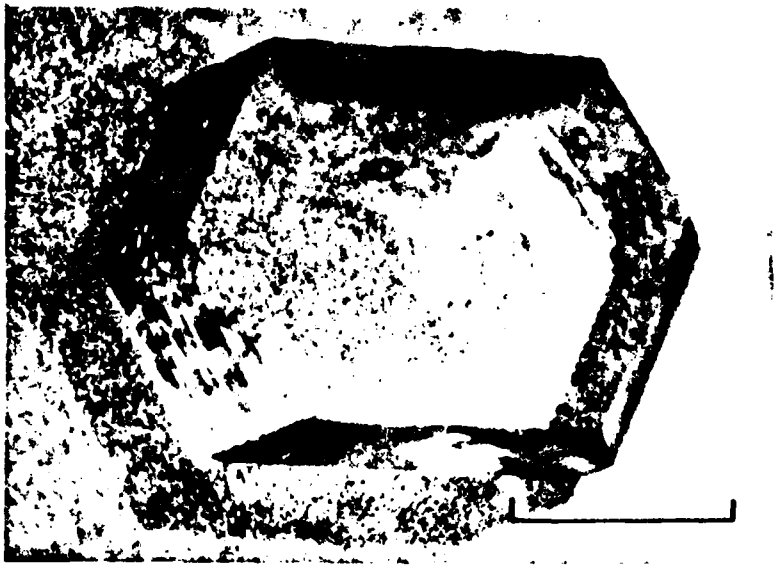

b

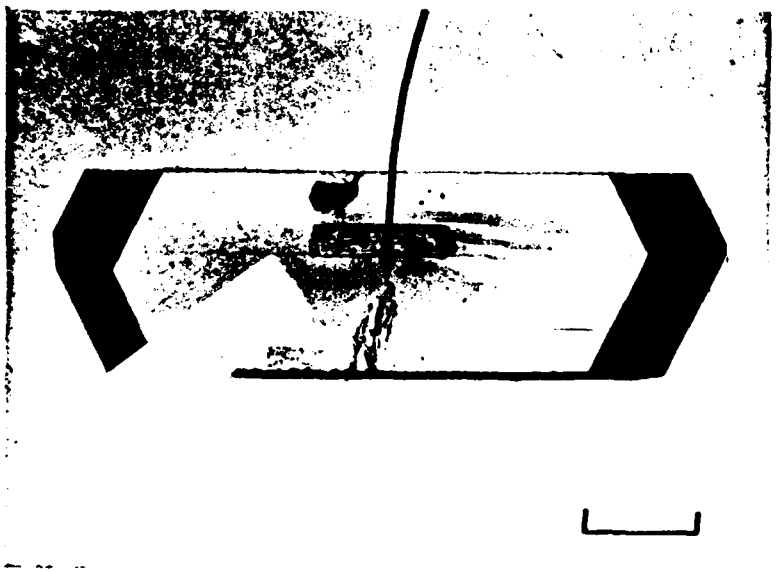

b

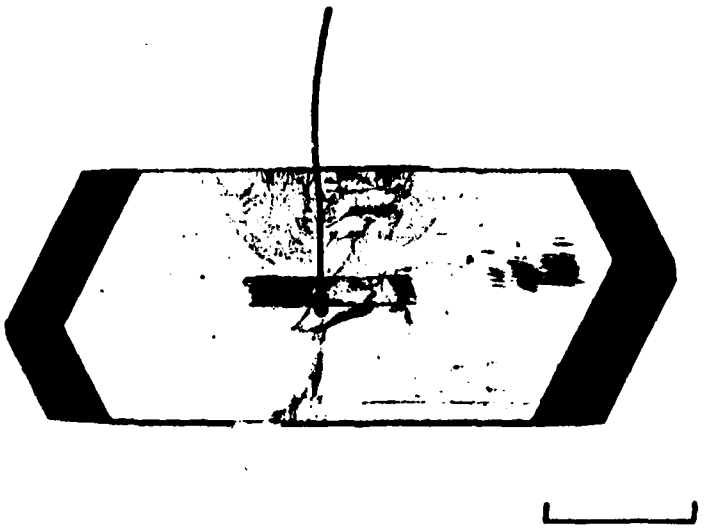

d

FIGURE 2

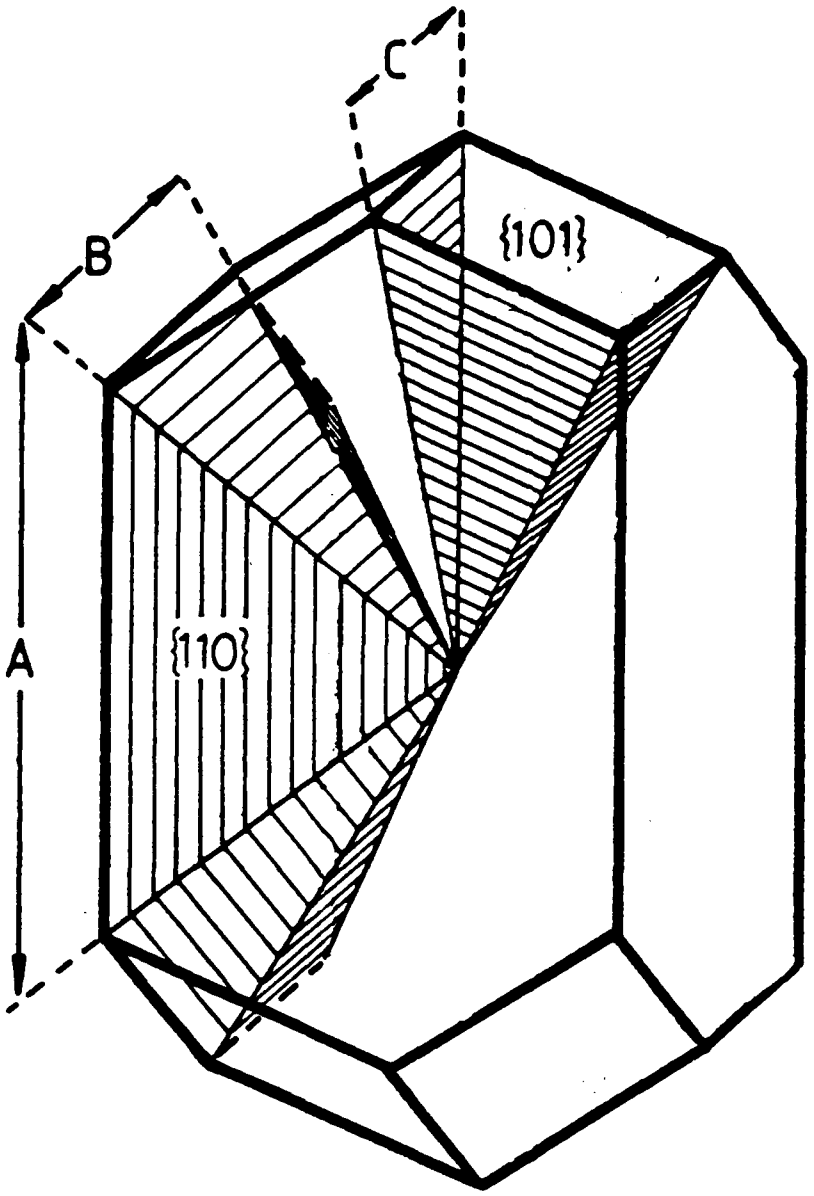

FIGURE 3

FIGURE 4

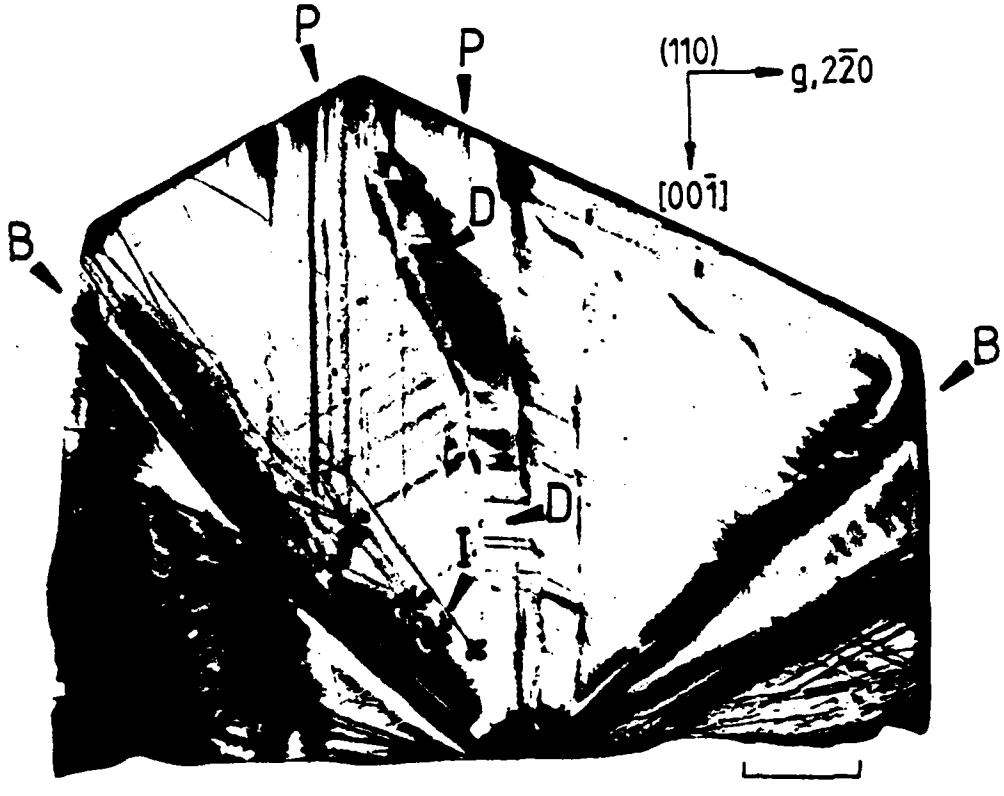

FIGURE 5

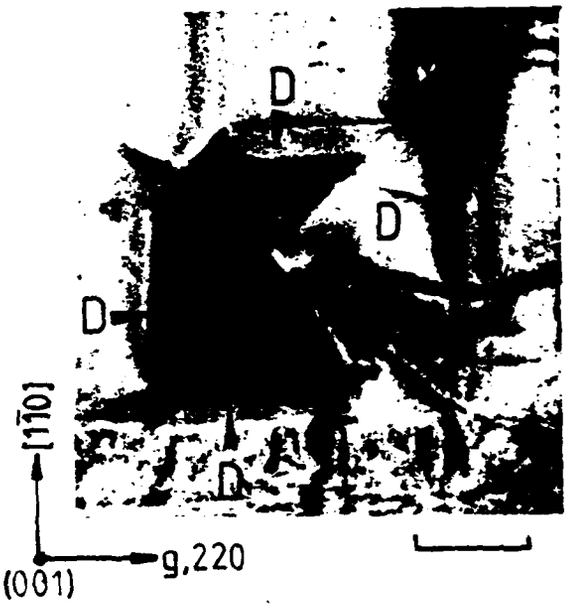

FIGURE 6

FIGURE 7

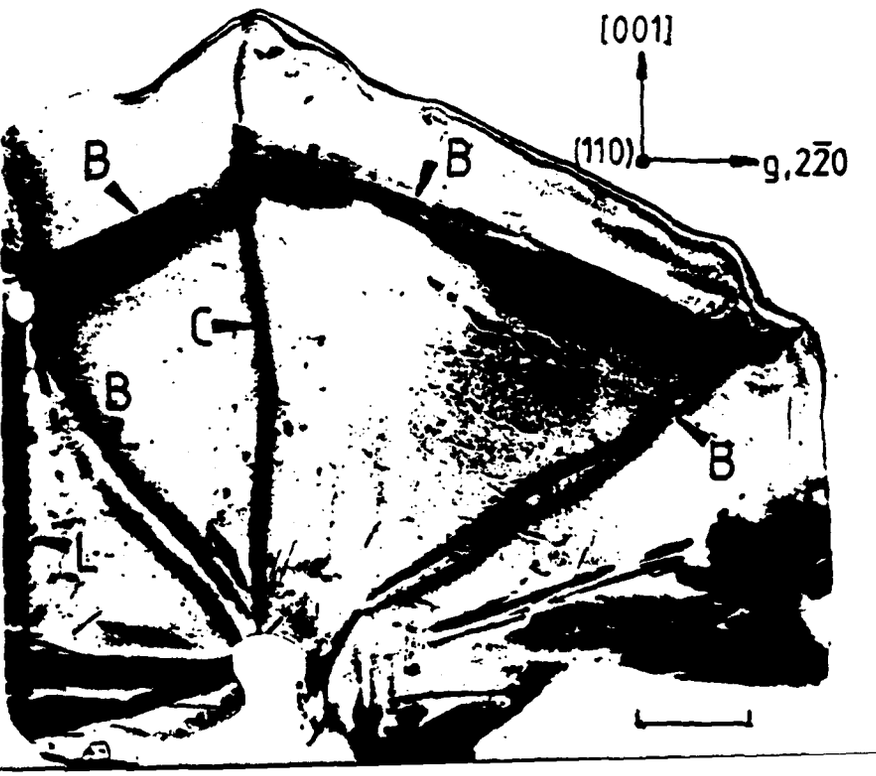

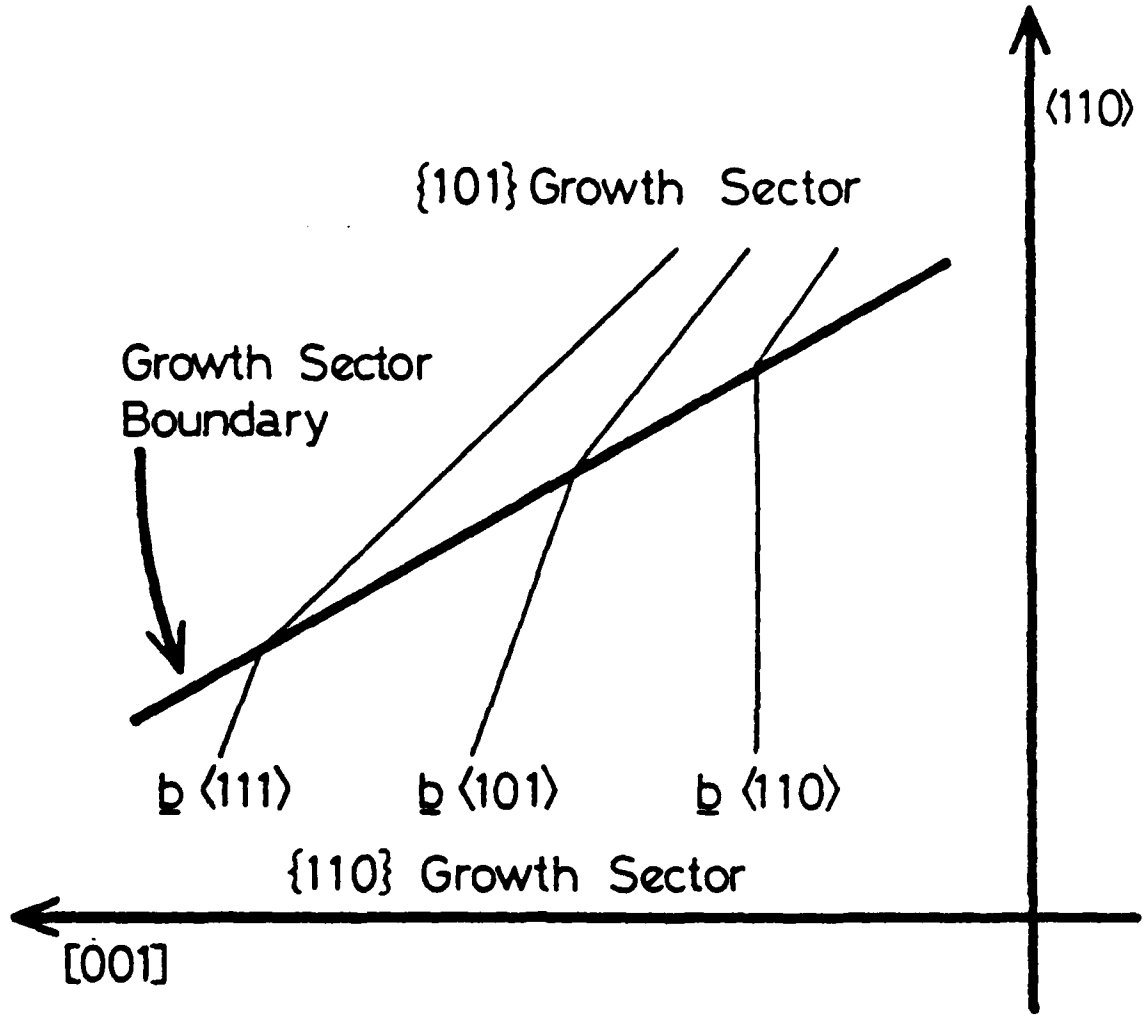
⟨110⟩
{101} Growth Sector
Growth Sector
Boundary
b ⟨111⟩
b ⟨101⟩
b ⟨110⟩
{110} Growth Sector
[001]

FIGURE 9

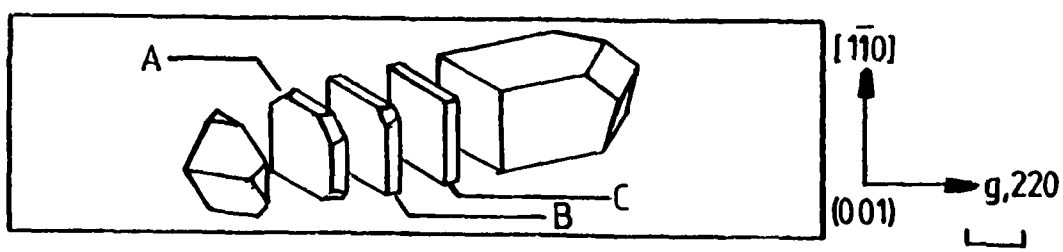

FIGURE 10

DISLOCATIONS IN ENERGETIC MATERIALS

2. Characterization of the Growth-Induced Dislocation Structure of Pentaerythritol Tetranitrate (PETN)

P.J. Halfpenny+, K.J. Roberts and J.N. Sherwood

Department of Pure and Applied Chemistry

University of Strathclyde

Glasgow G1 1XL

Current addresses:

+Engineering Materials Laboratories, University of Southampton, Highfield, Southampton SO9 5NH

ABSTRACT

The predominant dislocation types in crystals of pentaerythritol tetranitrate (PETN) grown from solution have been observed and characterized using transmission X-ray topography. The dislocation characterization, carried out by contrast variations, was aided and simplified by comparison of observed dislocation line directions with those calculated from the Theory of Preferred Line Directions of Klapper. With few exceptions, the dislocations observed were induced during growth. Eight different types were identified comprising all possible Burgers vectors up to and including <111>. Of these, one was pure edge,the remainder being of mixed character. The relative frequency of occurrence of the dislocation types is discussed, together with factors influencing dislocation contrast and characterization.

1. INTRODUCTION

Crystal defects, in particular dislocations, have been observed to play a significant role in such processes as crystal growth (Burton et al 1951, van Enckevort 1982, Hooper et al 1983), solid state polymerization (Meyer et al 1978), solid state decomposition (Thomas 1969, Thomas and Williams 1971, Herley and Levy 1972, Begg et al 1981, Monkowski 1981) and the performance of solid state devices (Meieran 1980). Speculations have also been made of their involvement in both the slow and rapid decomposition of energetic solids. Singh (1956) has observed the thermal decomposition of mercury fulminate to occur preferentially on (010) and (100) planes. He interpreted this in terms of a redistribution of dislocations on these planes during heating. Similarly, Jach (1962) proposed preferential decomposition at dislocations to account for the observed thermal decomposition kinetics of lead azide. A detailed understanding of the behaviour and properties of dislocations in crystalline explosives are of interest not only to qualify such speculations but also because it has been proposed that the initiation of explosives by impact may occur through the formation of localised 'hot spots' following plastic deformation (Bowden 1958; Elban and Armstrong 1981).

The properties of a dislocation are, in general, strongly dependent on its character and on whether or not it is formed during growth or induced mechanically at a later stage in growth. Dislocation characterization is therefore an important step towards understanding defect properties and relating these to the

behaviour of the bulk material. X-ray topography (Lang 1954) provides a useful tool in the analysis of growth-induced dislocation configurations in large, nearly perfect single crystals. Using this technique, we have determined the nature of the growth induced dislocation structure of the important organic secondary explosive pentaerythritol tetranitrate (PETN).

The basic method of characterization of dislocations by X-ray topography uses the invisibility criteria $\underline{g}.\underline{b} = 0$ and $\underline{g}.\underline{b} \times \underline{l} = 0$, where $\underline{g}$ is the diffraction vector and $\underline{b}$ and $\underline{l}$ are the Burgers vector and line vector respectively of the dislocation (Lang 1978). The method is frequently hindered by a number of factors.

1. The criteria apply strictly only to elastically isotropic media.

2. Mixed dislocations seldom become completely invisible. This is particularly significant in the analysis of growth dislocations which rarely follow low-indexed line directions and are often of mixed character.

3. Dislocations are often decorated by solvent or other im purities. This can modify the strain field of the dislocation thus making it visible in all reflections. This again can be a common occurrence with growth dislocations.

4. The unambiguous Burgers vector assignment of any dislocation requires invisibility or near invisibility in at least two reflections. Each reflection defines a plane in which the Burgers

vector lies and the line of intersection defines b itself. It is often the case that the particular reflection or reflections required are unavailable. This may be due to

a) Systematic absences

b) The required reflection may be too weak to give dislocation images suitable for analysis. This is a common problem with organic materials due to the small atomic scattering factors.

c) Some reflections will be inaccessible due to the geometry of the slice plane available.

5. Superimposition of defects causes difficulty in establishing whether or not a dislocation has become invisible.

As will be confirmed below several of these factors present problems in attempting a dislocation analysis in the present case. In several publications Klapper has shown that growth induced dislocations normally follow well-defined directions in crystals. He has developed a theory based on the linear anisotropic elastic properties of a defective lattice which confirms the observed orientations. In this paper we have used theoretical calculations of the preferred line directions in PETN to supplement the extinction contrast data. In this way a satisfactory determination of the character of the growth dislocation structure can be obtained despite the problems noted above.

2. THEORETICAL ANALYSIS OF GROWTH-INDUCED DISLOCATION TYPES

A preliminary topographic examination of PETN single crystals (Halfpenny et al 1984 a) has revealed that, almost without exception, the dislocations were straight and followed a number of discrete, well-defined line directions. Few of these line directions were low-indexed. Most dislocations originated from either inclusions or growth sector boundaries. Such features are characteristic of growth-induced dislocations (Klapper 1980).

As an aid to the characterization of these dislocations, it is valuable to consider the various growth dislocation families which might be expected to occur in PETN. This involves, firstly, establishing the probable Burgers vectors, $\underline{b}$. The line direction of a given growth dislocation is defined by its Burgers vector and the growth direction, $\underline{n}$, of the growth sector in which it lies. It is, therefore, also necessary to consider the possible combinations of $\underline{b}$ and $\underline{n}$.

2.1 Burgers Vectors

PETN crystallizes in the tetragonal space group $P\bar{4}2_1c$ with a = b = 0.938nm and c = 0.67nm (Booth and Llewellyn 1947). Since the unit cell is primitive there is no halving of lattice translations due to centring. For energetic reasons, the shorter lattice translations are generally favoured as dislocation Burgers vectors. On this basis Burgers vectors longer than <111>, although not completely discounted, were considered improbable. The shortest Burgers vectors for PETN are listed in Table 1.

2.2 Dislocation Families

Crystals of PETN exhibit the forms {110} and {101} only. Consequently there are twelve growth directions; four corresponding to the {110} growth sectors and eight to the {101} sectors. Together with the 13 probable Burgers vectors, this gives a total of 156 possible combinations of $\underline{b}$ and $\underline{n}$. In this instance the sense of the Burgers vector is unimportant since it does not influence the calculation of the line direction of the growth dislocation. Hence only 13, rather than the full 26 specific Burgers vectors up to and including <111> are considered. Many of the possible combinations of $\underline{b}$ and $\underline{n}$, and therefore the dislocation line directions they define, are symmetrically equivalent. The 156 possible combinations can be reduced to 16 non-equivalent combinations. These are listed in columns 2 and 3 of Table 2.

2.3 Calculation of Preferred Dislocation Line Directions

The potential configurations of dislocations in the growing crystal were evaluated using Klapper's theory. The calculation is based on linear anisotropic elasticity theory with the following basis.

The preferred line direction of a particular dislocation corresponds to that in which the dislocation energy per unit growth length is a minimum i.e.

$$W = \frac{E}{\text{Cos } \alpha} \text{ is a minimum}$$

where E is the dislocation energy per unit length of straight dislocation and α is the angle between the line vector $\underline{l}$ and the growth normal $\underline{n}$.

The energy of a linear dislocation consists of two terms, the elastic energy E_a of the long-range strains surrounding a dislocation and the dislocation core energy E_c. The former is given by

$$E_a = \frac{K|\underline{b}|^2}{4\pi} \ln \frac{R}{r_o}$$

where K is an energy factor which depends on $\underline{l}$, $\underline{b}$ and the elastic properties of the crystal. R and r_0 are the outer and inner cut off radii of the dislocation concerned. The core energy of dislocations cannot be calculated with any degree of accuracy. It can be neglected without serious error however, since it is usually estimated to be at least an order of magnitude smaller than E_a. Hence the dislocation energy per unit growth length can be written as

$$W = \frac{E_a}{\text{Cos } \alpha} = \frac{K}{\text{Cos } \alpha} \frac{|\underline{b}|^2}{4\pi} \ln \frac{R}{r_o}$$

For a given $\underline{b}$ the term in $\frac{R}{r_o}$ (typically $\sim$ 1.3) is independent of the line direction and the preferred line direction for a dislocation can then be obtained from the condition that

$$\frac{K}{\text{Cos } \alpha} \text{ is a minimum}$$

In order to find the position of this minimum for a particular dislocation, the dependence of $K/\cos\alpha$ on the line direction has to be determined.

The energy factor K was calculated using the linear anisotropic elastic theory of straight dislocations developed by Eshelby, Read and Shockley (1953) and detailed by Hirth and Lothe (1968). In the general case of anisotropy, since K cannot be expressed analytically, calculations were carried out numerically with the aid of a computer using Klapper's programme DISLOC (Klapper 1972ab). The following values of the elastic constants (in GPa) for PETN were used in the calculation (Morris 1976).

$C_{11} = 17.18$; $C_{12} = 5.43$; $C_{13} = 7.48$; $C_{33} = 12.14$;

$C_{44} = 5.03$; $C_{66} = 3.93$.

The results of the calculations are shown in Table 2. The calculated line directions are defined by two coordinates: θ and ϕ. θ is the angle between the dislocation and [001] while ϕ is the angle between [010], and the projection of the dislocation line in the (001) plane. The term ΔW is a qualitative indication of the sharpness of the dislocation energy minimum, normalised to the sharpest minimum (Type 3b dislocation, see table 2) as unity, i.e. the sharper the energy minimum, the greater the probability that the observed line direction will lie along the direction of minimum energy. These results define the sixteen theoretically possible growth dislocation families which may exist in PETN. Each preferred line direction is representative of its dislocation family and all

symmetrically equivalent line directions can easily be deduced from each unique configuration. The results of this analysis are summarized in Table 2.

3. EXPERIMENTAL CHARACTERIZATION OF DISLOCATION CONFIGURATIONS

3.1 Preparation of Samples for X-ray Topography

Crystals of PETN were grown from acetone and from ethyl acetate solutions by slow solvent evaporation and by temperature lowering (Hooper, McArdle, Narang and Sherwood 1980). These crystals were typically 30 x 10 x 10mm^3 and exhibited the forms {110} and {101} with the former dominant. The growth and perfection of PETN crystals is discussed in detail elsewhere (Halfpenny et al 1983a). The crystals were sectioned parallel to (110) using a solvent saw and the resulting slices polished on a solvent soaked cloth to a thickness (t) of about 1mm. Cyclohexanone was found to be the most effective solvent for both slicing and polishing.

3.2 X-ray Topography

Transmission X-ray topographs were recorded on a Lang camera using Cu$K\alpha_1$ radiation (0.154 nm). For this wavelength the linear absorption coefficient, μ, for PETN is 1.64 x 10^3 m^{-1}. Thus the product μt was approximately 1.5. The images were recorded on Agfa Structurix D4 X-ray film.

3.3 Characterization Procedure

The selection of X-ray reflections for the dislocation characterization was guided by the need for both extinction contrast and definition of the dislocation line directions. In the former case reflections were chosen such that the product $\underline{g}.\underline{b}$ should be zero for each likely Burgers vector. For some dislocations, unambiguous characterization was possible on the basis of this information alone. When a dislocation became invisible in fewer than two reflections, the characterization was completed by comparison of the observed and calculated line directions. Suitable reflections were found to be of the 200, 020, 220, 211, 121 and 222 types. In assessing the line directions full account was taken of projection distortion.

4. RESULTS OF THE DISLOCATION CHARACTERIZATION

Table 3 summarizes the predominant growth dislocation types observed and characterized in PETN. The reference numbers and letters refer to the dislocation types listed in Table 2. Eight examples (labelled A to G in the following figures) have been selected to illustrate this characterization. The geometry of the slice containing dislocations A to C and E to G is shown schematically in Figure 1. Figures 2 a-f are X-ray topographs of this slice. Dislocation D is shown in Figure 3. The observed and calculated dislocation line directions for the dislocations in various reflections, are listed in Table 4. These examples comprise all dislocation types observed in a wide range of crystals examined.

We have subdivided these eight characterizations into three loose groupings. First we describe those dislocations which can be characterized completely by extinction contrast experiments. We show that the dislocation line directions are in full agreement with those theoretically predicted and thus verify the applicability of this theory to the analysis of growth-induced dislocations in PETN. Second, we combine extinction contrast experiments with analysis from preferred line directions in cases where characterization by the former technique did not provide an unambiguous characterization. Third, we apply the theoretical predictions to the case of dislocations which offer no extinctions for analysis by contrast considerations. In addition to this we note the qualitative information which can be gained from the dislocation images without use of the theoretical results.

4.1 Characterization from Extinction Contrast Experiments

Dislocation A

The dislocations labelled A in Figure 1 lie in the $(\bar{1}10)$ growth sector. They are normal to the $(\bar{1}10)$ face which indicates they are probably pure edge or pure screw in character. This information limits the possible Burgers vectors to [001], [110], [111] or $[11\bar{1}]$. Beyond this, the dislocation line directions provide no further information. The dislocations are invisible in the $\bar{2}00$, $0\bar{2}0$ and $2\bar{2}0$ reflections. The only Burgers vector which satisfies the condition $\underline{g}.\underline{b} = 0$ for each of these diffraction vectors is [001]. Dislocations A are thus characterized as type 1a (dislocation types noted in this section refer to Table 2) with

Burgers vector [001] in the $(\bar{1}10)$ growth sector and are therefore pure edge in character.

Dislocation B

Dislocation B is in the $(\bar{1}0\bar{1})$ growth sector. Since it is not parallel to the growth direction it is probably mixed in character. It is also relatively short which shows that it lies at a fairly high angle to the slice plane. The dislocation is invisible in the $\bar{2}00$, $0\bar{2}0$ and $2\bar{2}0$ reflections which again indicates the Burgers vector to be [001]. The dislocation also shows weak contrast in many other reflections. The characterization by invisibility only is consequently far from conclusive but is confirmed by good agreement of observed and calculated line directions. Dislocation B is therefore characterized as type 1b and is, as expected, mixed.

Dislocation E

Dislocation E in Figure 1 is relatively long which suggests that it lies parallel to or at only a low angle to the slice plane. This, together with its projected line direction shows that it is not parallel to the growth direction and is again of mixed character. The dislocation is invisible in both the $1\bar{2}\bar{1}$ and $2\bar{2}\bar{2}$ reflections. The only Burgers vector satisfying the condition $\underline{g}.\underline{b} = 0$ in both cases is [101]. The observed and calculated line directions for this Burgers vector in the $(0\bar{1}1)$ growth sector also give good agreement as shown in Table 4. Dislocation E is therefore characterized as type 3c with Burgers vector [101] in the $(0\bar{1}1)$ growth sector.

4.2 Characterization from a Combination of both Extinction Contrast and Preferred Line Directions

Dislocation C

The dislocation C has the same projected line direction as A in many of the reflections. In the highly asymmetric $\bar{2}\bar{1}\bar{1}$ reflection, however, the difference in their true line directions is defined. Since A and C lie in the same growth sector and have different line directions, it follows that their Burgers vectors are different. As dislocation C does not lie parallel to the growth direction, it is probably mixed. It is invisible in the $0\bar{2}0$ reflection only. The Burgers vectors consistent with this result are [001], [100], [101] and [$\bar{1}$01]. [001] is eliminated by the argument above (i.e. it is not A).

The dislocation is therefore characterized as type 2a with a Burgers vector [100] and lies in the ($\bar{1}$10) growth sector.

Dislocation G

Dislocation G exhibits a sharp change in line direction as it passes from the ($\bar{1}$01) to the ($\bar{1}$10) growth sector. Its Burgers vector must remain the same however. Both parts of the dislocation G_1 and G_2 in the ($\bar{1}$01) and ($\bar{1}$10) sectors respectively are mixed since they do not lie along the growth normal in either case. The dislocation is invisible in the $\bar{2}\bar{1}\bar{1}$ reflection only. Its Burgers vector may therefore be either [$\bar{1}$11] or [0$\bar{1}$1]. The

Only $[\bar{1}11]$ gives good agreement between observed and calculated line directions for both growth sectors. Dislocation G is therefore of type 5a in the $(\bar{1}10)$ sector (G_2) and of type 5c in the $(\bar{1}01)$ sector (G_1).

4.3 Characterization from only the Preferred Line Direction

Dislocation D

Dislocation D in Figure 3 makes a large angle with the growth direction of the $(10\bar{1})$ growth sector in which it lies. It is therefore of mixed character. It did not become invisible in any reflection and consequently could not be characterized by the g.b criterion. Examination of the calculated line directions for the $(10\bar{1})$ growth sector showed that only the Burgers vector [100] gave a line direction even remotely near to that observed. This Burgers vector gives good agreement between observed ($\theta = 60°$) and calculated ($\theta = 57°$) line directions. Dislocation D is therefore characterized as type 2b with Burgers vector [100] in the $(10\bar{1})$ sector and is of mixed character. It is noteworthy that no information about the Burgers vector of this dislocation could have been obtained without the calculated line direction.

Dislocation F

The dislocations labelled F have the same projected line direction as E in the $2\bar{2}0$ reflection. Their shorter length however suggests that they lie at a larger angle to the slice plane than the latter. The difference in projected line directions in other reflections confirms this. As discussed earlier, since they lie

in the same growth sector, dislocations E and F must therefore have different Burgers vectors. Dislocations F remain visible in all accessible reflections which again precludes characterization by the invisibility criteria. Comparison of observed and calculated line directions gives good agreement for a Burgers vector of [110] (type 4c) in the (011) growth sector. They are of mixed character.

5. DISCUSSION

5.1 Basic Growth-Induced Dislocation Structure

The number of dislocations of each type within different samples was found to vary considerably with the crystal perfection. Consequently the relative frequency of occurrence of each type can only be discussed in very general terms. From the twenty crystals examined, however, the following observations became apparent. Firstly, dislocations of types 1b, 2b. 3c. 4c and 5c, i.e. all those occurring in {101} growth sectors, were less common

than the remaining types. The crystal slice shown in Figure 3 is almost devoid of dislocations in one of the {101} sectors. Where dislocations occurred in large numbers in these sectors, however, those of types 3c and 5c were usually dominant. Of the dislocations occurring in {110} sectors, those of type 5a were by far the most common with type 1a dislocations also present in significant numbers.

It is interesting to recall that growth dislocations in PETN have been observed, having Burgers vectors up to and including <111>. No evidence has been found for dislocations of larger Burgers vectors. The elastic line energies of those observed, range from 19 to 83eVnm^{-1}. The growth dislocations are clearly not confined to those of lowest line energy. In fact the most commonly occurring dislocation type is that of highest line energy. Dislocations with large line energies have also recently been observed in single crystals of ammonium dihydrogen orthophosphate (Bhat et al. 1983). These observations suggest that the line energy of a given dislocation is not necessarily the controlling factor in determining whether or not the dislocation occurs.

Bearing in mind the manner in which growth dislocations are formed, i.e. at inclusions or at disturbed regions of the crystal such as the seed, the most significant factor in determining the Burgers vector is probably the nature of the misorientation at which the dislocation is nucleated.

5.3 Dislocation Motion and Mechanically Induced Dislocations

It is interesting to note that the dislocations observed in PETN exhibited an almost exclusive linear line direction with no evidence for dislocation motion either during or after growth. Etching and microhardness indentation studies of PETN (Halfpenny et al. 1984b) have shown that the material is comparatively soft (surface hardness 17kgm^{-2}) and readily undergoes slip on the {110} planes. The lack of glide-induced motion of most growth dislocations could be explained by their potentially sessile nature (with the exception of type 1a) i.e. the fact that $\underline{l}$ and $\underline{b}$ do not lie in the dominant {110} slip planes. In contrast, dislocations of type 1a (Edge type $\underline{l}$ = [110], $\underline{b}$ = [001]) certainly should slip. That they do not do so could reflect the fact that rather low mechanical stresses develop in the crystals during growth.

A further observation which could also explain the lack of motion is our difficulty in obtaining extinction conditions for dislocations in this material. This could well reflect a high level of impurity or, more probably, solvent decoration of dislocations. In addition to causing the observed effect, this could also result in dislocation pinning and hence restriction of migration by either slip or climb. We believe that either of these possibilities could perhaps explain the lack of dislocation motion in this solid.

6. CONCLUSIONS

This study shows the utility of Klapper's Theory of Preferred Dislocation Line Directions as an aid in the provision of complete and comprehensive analysis of growth-induced dislocation structure in single crystals. Using, initially, a combination of extinction contrast criteria and preferred line directions we verify the applicability of this theory in the case of the energetic solid PETN. Latterly, we are thus able, on dislocation line direction data alone, to characterize many dislocations of mixed character whose Burgers vectors we cannot unambiguously define using extinction contrast criteria.

Eight families of dislocations with Burgers vectors [001], <100>, <101>, <110> and <111> are observed in single crystals of PETN. Dislocations with the *long* Burgers vector <111> are found to predominate in the dislocation structure suggesting that the line energy is not the dominant factor in dislocation formation. All of the dislocation types, with one exception which is an edge dislocation, are of mixed character. This solid exhibits no direct evidence for growth-induced dislocation motion by either glide or climb mechanisms. This we attributed to the mostly sessile nature of the dislocations observed, together with a likelihood of solvent-impurity pinning of the dislocations.

ACKNOWLEDGEMENTS

We express our grateful thanks to the European Office of the US Army (USARDSG-UK) for their financial support of this work. We are also grateful to Professor H. Klapper (RWTH Aachen, FRG) for his provision of a copy of the computer programme DISLOC and for subsequent helpful discussions.

REFERENCES

I.D. Begg, K.J. Roberts, J.N. Sherwood, I. Groth-Andersen and C.S. Jacobsen, 1981, Chem. Phys. Lett. 79, 513.

I.D. Begg, P.J. Halfpenny, R.M. Hooper, R.S. Narang, K.J. Roberts and J.N. Sherwood, 1983, Proc. Royal Soc. A 386 431.

H.L. Bhat, K.J. Roberts and J.N. Sherwood, 1983, J. App. Cryst., 16, 390.

A.D. Booth and F.J. Llewellyn, 1947, J. Chem. Soc., 837.

F.P. Bowden, 1958, Proc. Royal Soc. A 246, 146.

W.K. Burton, N. Cabrera and F.C. Frank, 1951, Phil. Trans. Royal Soc., A 243 299.

W.C. Dash, 1957, Dislocations and the Mechanical Properties of Crystals, Wiley, New York, p57.

W.L. Elban and R.W. Armstrong, 1981, 7th International Symposium on Detonation, Annapolis, Maryland 1981.

J.D. Eshelby, W.T. Read and W. Shockley, 1953, Acta Met. 1, 251.

P.J. Halfpenny, K.J. Roberts and J.N. Sherwood, 1984a, (Part 1) J. Crystal Growth, in press.

P.J. Halfpenny, K.J. Roberts and J.N. Sherwood, 1984b, (Part 3), J. Material Sci., in press.

P.J. Herley and P.W. Levy, 1972, Reactivity of Solids, Ed. J.S. Anderson, M.W. Roberts and F.S. Stone, Chapman and Hall, London, p387.

J.P. Hirth and J. Lothe, 1968, Theory of Dislocations, McGraw-Hill, New York, p399.

R.M. Hooper, B.J. McArdle, R.S. Narang and J.N. Sherwood, 1980, Crystal Growth'. Second Edition Ed. B.R. Pamplin, Pergamon, Oxfor p395.

R.M. Hooper, K.J. Roberts and J.N. Sherwood, 1983, J. Materials Sci., 18, 81.

J. Jach, 1962, Nature, 196 827.

A.E. Jenkinson and A.R. Lang, 1962, Direct Observation of Imperfections in Crystals, Ed. Newkirk and Wernick, Wiley, New Yor p471.

H. Klapper, 1972a, Phys. Stat. Sol. a, 14, 79.

H. Klapper, 1972b, Phys. Stat. Sol. a, 14, 443.

H. Klapper, 1975, Habilitationsschrift, RWTH, Aachen.

H. Klapper, 1980, Characterization of Crystal Growth Defects by X-ray Methods, Eds. B.K. Tanner and D.K. Bowen, Plenum, New York, p122.

A.R. Lang, 1959, J. Appl. Phys., 30, 1748-1755.

E.S. Meieran, 1980, Characterization of Crystal Growth Defects by X-ray Methods, Ed. B.K. Tanner and D.K. Bowen, Plenum, New York, p1.

W. Meyer, G. Lieser and G. Wegner, 1978, J. Polymer Sci. Polymer Phys., 16, 1365.

J.R. Monkowski, 1981, Solid State Technol., 24 44.

C.E. Morris, 1976, 6th Symposium on Detonation

K. Singh, 1956, Trans. Faraday Soc., 52, 1623.

G.K. Stokes, S.R. Keown and D.J. Dyson, 1968, J. App. Cryst, 1, 68.

J.M. Thomas, 1969, Adv. in Catalysis, 10, 293.

J.M. Thomas and J.O. Williams, 1971, Prog. Sol. State Chem., 6, 119.

W.J.P. van Enckevort, 1982, Doctoral Thesis, University of Nijmegen.

Whittaker, 1981, Crystallography, Pergamon, Oxford, p36.

FIGURE CAPTIONS

Figure 1 Schematic representation of crystal 1

(a) Location of the various dislocation types referred to in the text.

(b) Crystallographic geometry of slice A showing the locations of the various growth sectors. The inset gives the principle crystal axis.

(c) The position of the slice on the original crystal.

Figure 2 Transmission X-ray topographs of crystal 1.
The diffraction geometry, in each case, is shown in the inset. The reflections are: (a) $2\bar{2}0$; (b) $0\bar{2}0$; (c) $\bar{2}00$; (d) $\bar{2}1\bar{1}$; (e) $1\bar{2}\bar{1}$; (f) $2\bar{2}\bar{2}$.

Figure 3 Transmission X-ray topograph of crystal 2.
The slicing plan and diffraction geometry is shown in the inset. $2\bar{2}0$ Reflection.

TABLE 1

PETN BURGERS VECTORS

$\underline{b}$	$\underline{\lvert b \rvert}$
uvw	nm
[001]	0.67
<100>	0.938
<101>	1.153
<110>	1.327
<111>	1.486

Type	$\underline{b}$	Growth Sector	Angle Between $\underline{b}$ and $\underline{n}$	Character	ϕ	θ	ΔW^{+}	E $eVnm^{-1}$	% Screw Component
1a	[001]	(110)	90	Edge	45	90	0.6	19	0
1b		(101)	35.5	Mixed	90	34	0.5	18	97
2a	[100]	(110)	45	Mixed	67	90	0.8	35	70
2b		(101)	54.5	Mixed	90	58	0.9	35	71
2c		(011)	90	Edge	0	36	0.3	46	0
3a	[101]	(110)	54.9	Mixed	66	70	0.9	47	67
3b		(101)	19	Mixed	90	50	1.0	42	91
3c		(011)	61.7	Mixed	47	40	0.7	52	51
3d		(10$\bar{1}$)	90	Edge	90	144	0.3	69	0
4a	[110]	(110)	0	Screw	45	90	0.4	77	100
4b		($\bar{1}$10)	90	Edge	315	90	0.7	85	0
4c		(101)	54.9	Mixed	75	49.5	0.5	81	47
5a	[111]	(110)	26.8	Mixed	45	69.5	0.7	84	89
5b		(1$\bar{1}$0)	90	Edge	135	90	0.7	103	0
5c		(101)	39.1	Mixed	69	47	0.9	82	68
5d		(10$\bar{1}$)	90	Edge	90	144	0.4	118	0

TABLE 2

PREFERRED DISLOCATION LINE DIRECTIONS IN PETN

$^{+}$Values of $\Delta W/10^{10}$ Nm^{-2} are normalised to the sharpest minimum in the set (type 3b dislocations).

TABLE 3

OBSERVED DISLOCATION TYPES IN PETN

Type	$\underline{b}$	Growth sector
1a	[001]	{110}
1b	[001]	{101}
2a	<100>	{110}
2b	<100>	{101}
3c	<101>	{011}
4c	<110>	{101}
5a	<111>	{110}
5c	<111>	{101}

Dislocation	A		B		C		D		E		F		G_2		G_1	
	1a		1b		2a		2b		3c		4a		5a		5c	
Reflection	Obs	Calc	Obs	Calc	Obs	Calc	Obs	Calc	Obs	Calc	Obs	Calc	Obs	Calc	Obs	Calc
$2\bar{2}0$	-	-	-	-	90	90	60	57	38	36	36	34	69	68	44	47
$1\bar{2}\bar{1}$	90	90	160	156	88	88	-	-	-	-	43	46	70	70	41	44
$0\bar{2}0$	-	-	-	-	-	-	-	-	36	34	45	50	62	65	obscured	
$\bar{2}00$	-	-	-	-	90	90	-	-	31	35	31	27	65	66	49	47
$00\bar{2}$	90	90	154	156	95	100	-	-	40	42	53	58	69	72	52	55
$2\bar{2}\bar{2}$	94	96	150	144	88	88	-	-	-	-	33	33	47	45	47	45

TABLE 4

OBSERVED AND CALCULATED* LINE DIRECTIONS OF DISLOCATIONS A to G

*Calculated values refer to the projected angle θ of the dislocation types specified in Table 2.

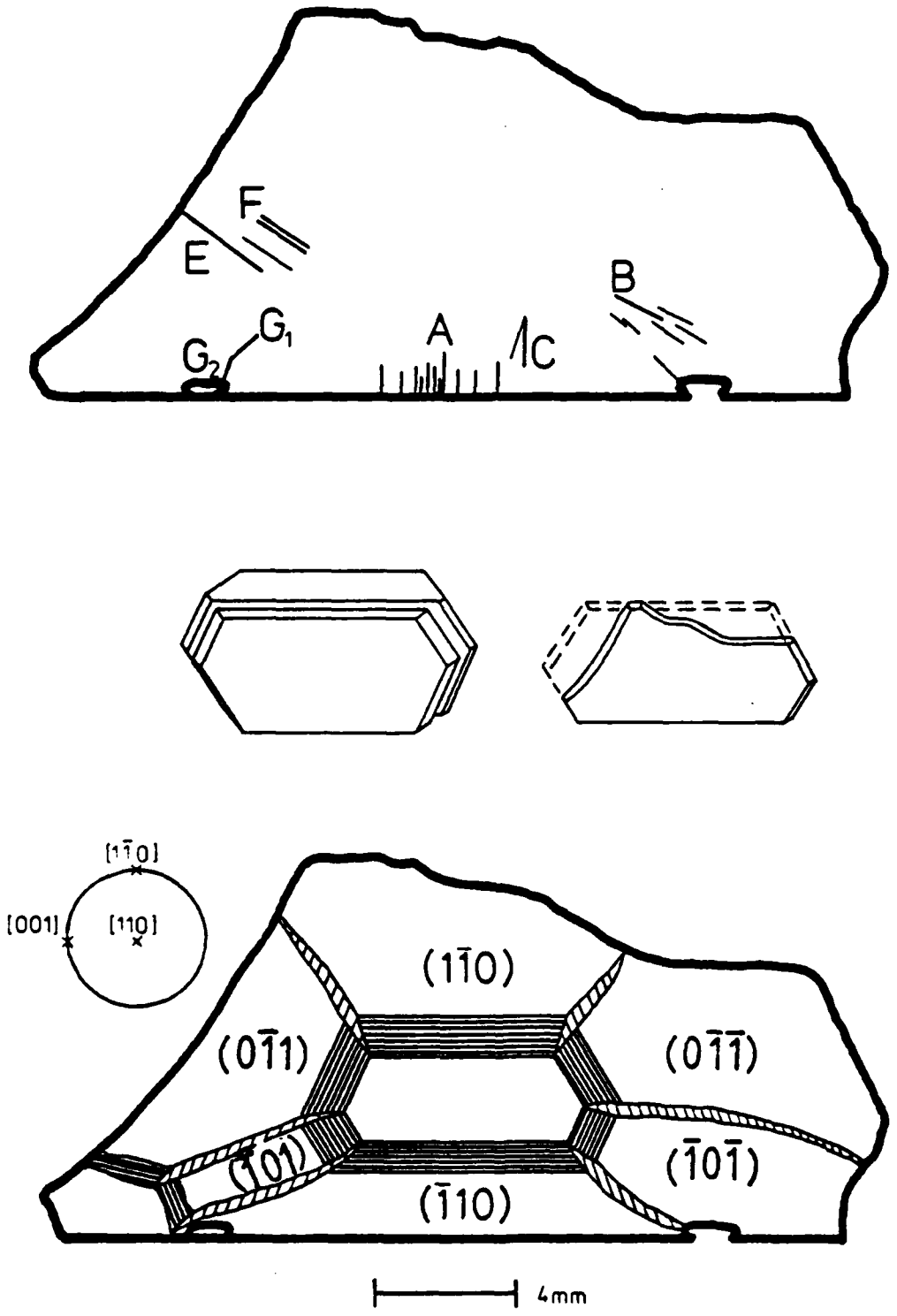
F
E
B
G1
G2
A
C
[1$\bar{1}$0]
[001]
[110]
(1$\bar{1}$0)
(0$\bar{1}$1)
(0$\bar{1}$$\bar{1}$)
($\bar{1}$01)
($\bar{1}$0$\bar{1}$)
($\bar{1}$10)
4mm

FIGURE 1

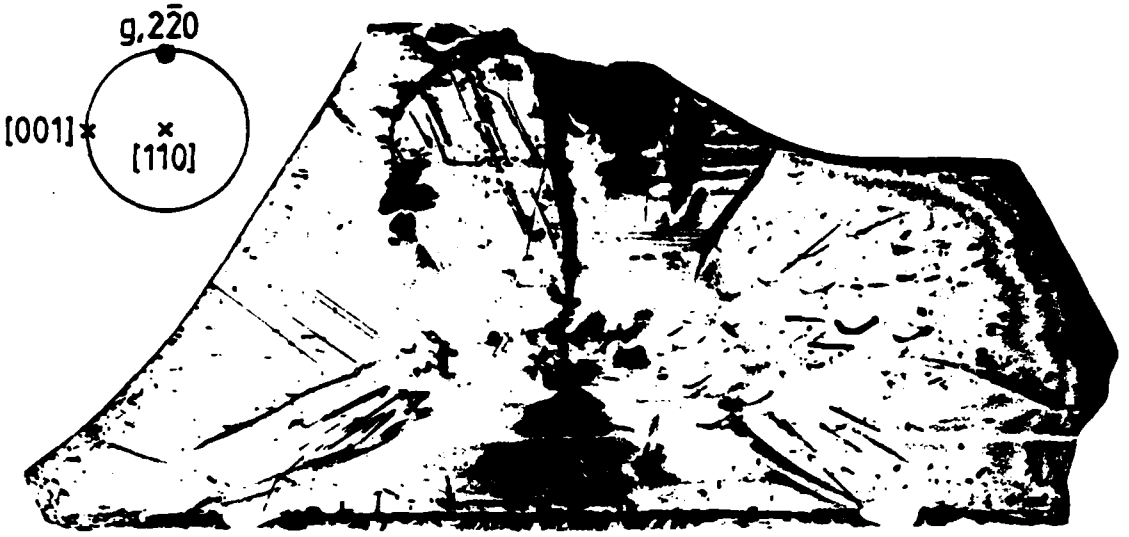

FIGURE 2a

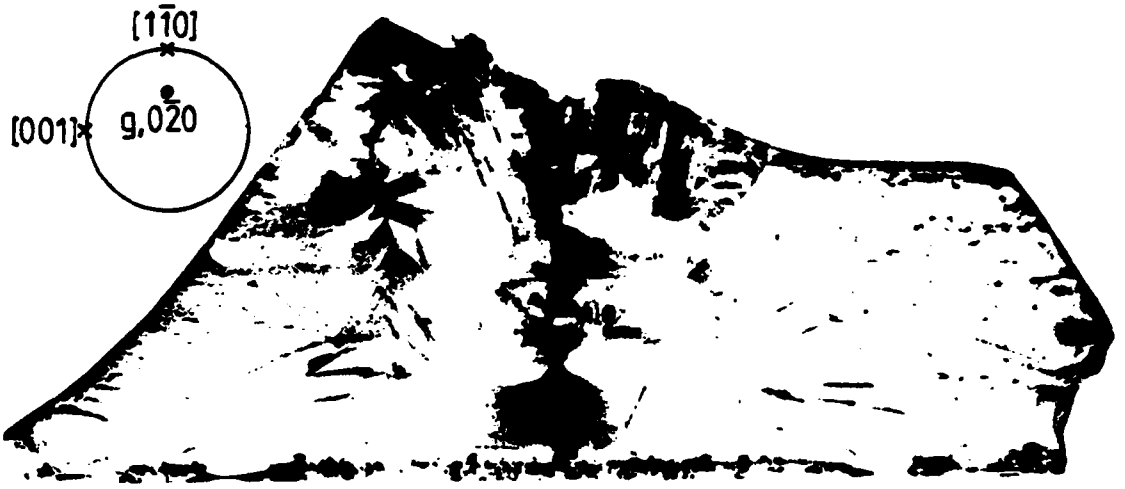

FIGURE 2b

FIGURE 2c

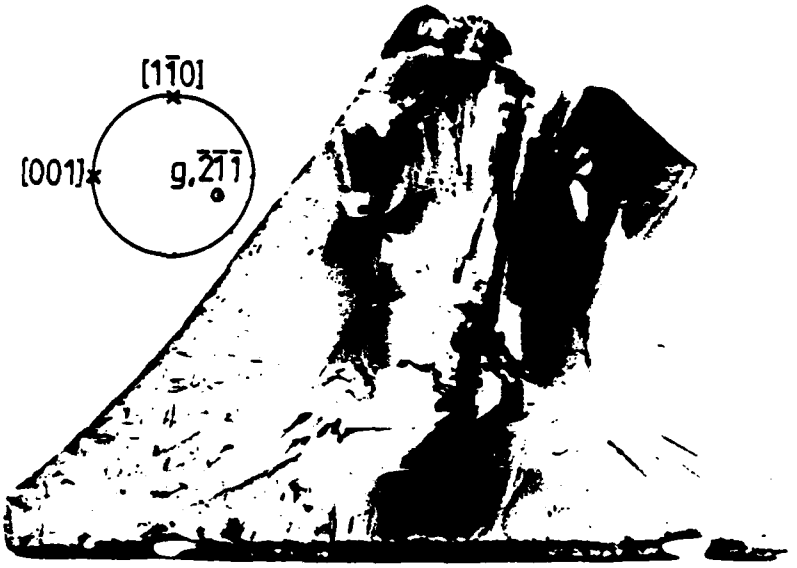

FIGURE 2d

FIGURE 2e

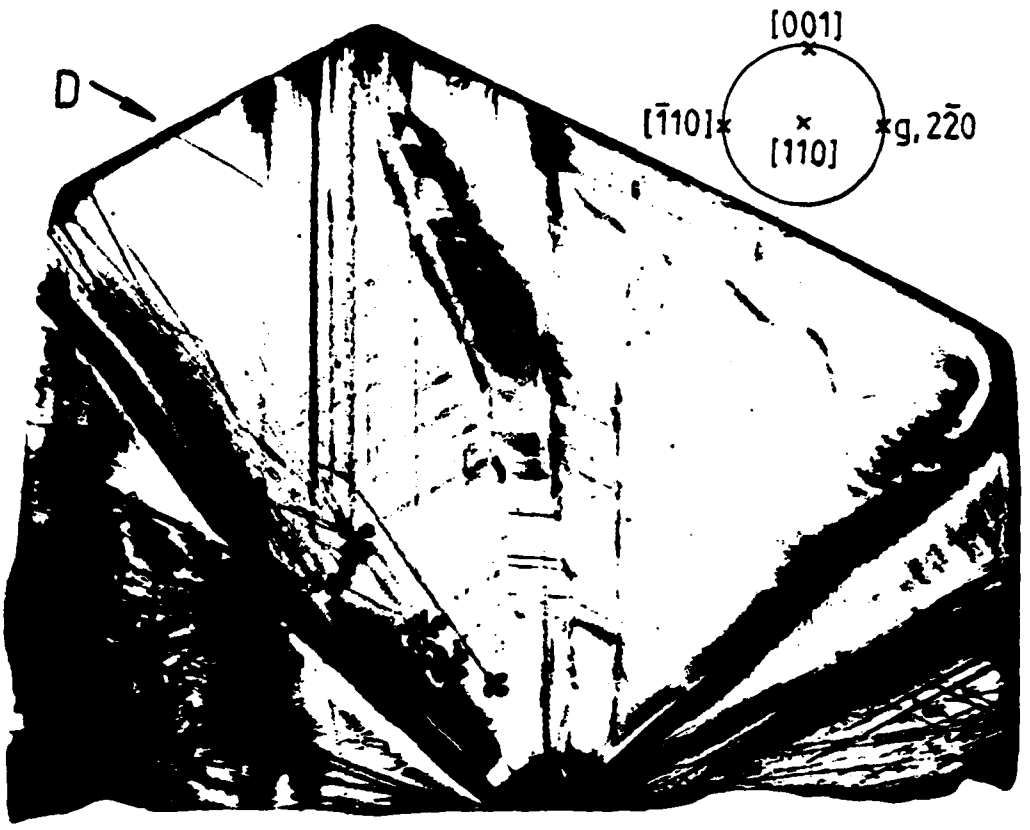

FIGURE 3

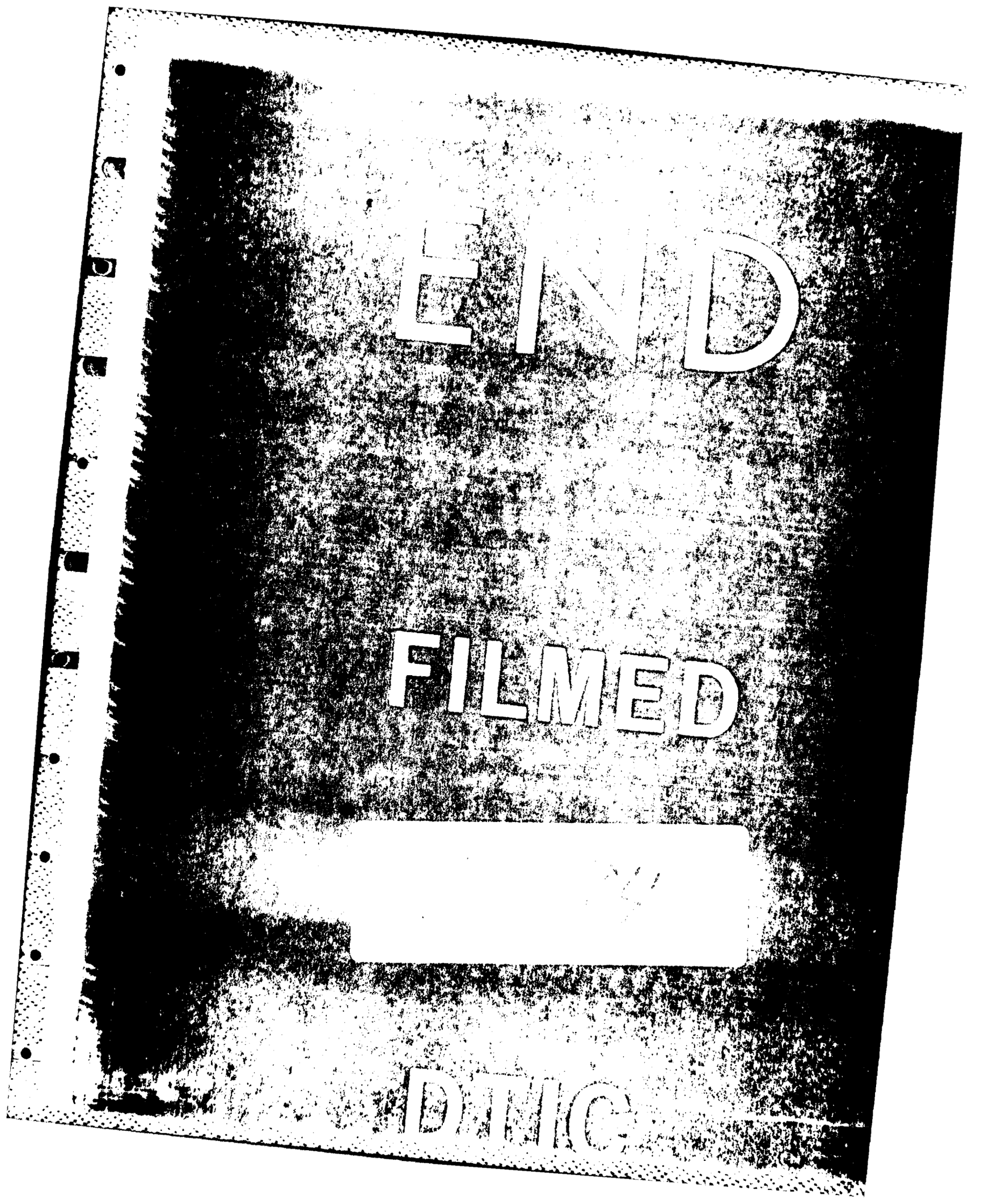
END
FILMED
DTIC